Flexible and Stretchable Strategies for Electronic Skins: Materials, Structure, and Integration

Zuqing Yuan, Su-Ting Han, Wenchao Gao,* and Caofeng Pan*

Cite This: *ACS Appl. Electron. Mater.* 2022, 4, 1−26

Read Online

ACCESS | Metrics & More | Article Recommendations

ABSTRACT: The basic materials, designs, and integration strategies have accelerated the significant development of electronic skins (E-skins). E-skins can transform skin-like sensory stimulations into various types of information. They have been utilized for wearable devices, robotics, human—machine interfaces, and prosthetics. However, there are still challenges for E-skins to support complex and subtle recognition. This review discusses the materials, structural designs, and integrated techniques for E-skins. We first introduce the common materials to fabricate E-skins. Then, we discuss the sensing mechanisms and structural engineering to establish a tactile sensor. An emphasis on how to optimize the performance is also discussed. Following that, we introduce representative progress in E-skins and focus on their integration strategies and applications. Future challenges and possible opportunities in the E-skins are discussed in the conclusion.
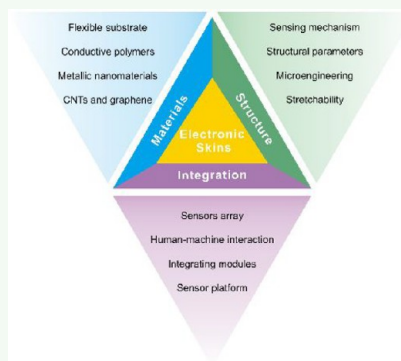
1. INTRODUCTION

With the development of electronic science and technology, flexible and portable electronics have become indispensable tools of social life.[1−4] Researchers try to find better solutions to establish a new combination of people, data, processes, and all. These factors make connections more relevant and valuable in the new area of Internet of Things (IOTs).[5−7] The basic materials, designs, and integration techniques of electronic devices have accelerated considerable development in IOTs, mainly because of nanomaterials and flexible electronics.[6,8−14] As one of the essential flexible electronics, E-skin can transfer the skin-like sensory stimulation and information to machines.[15−18] By recognizing the information from environments and humans themselves, E-skins will bring richer experiences to satisfy daily and industrial requirements.

The skin is the largest organ in the human body and possesses various excellent properties, including stretchability, toughness, self-healing, tactile sensation, and other sensing capabilities. E-skins mimic human skins to accept and transfer sensory stimulation information. They have been in the fields of wearable devices, robotics, human-machine interfaces (HMIs), and prosthetics. However, there are still challenges in achieving stable, comfortable, and multifunctional E-skins to support complex and subtle recognition.[19−22] Furthermore, when connecting to surroundings, machines rely on convenient, low-cost, and sensitive E-skins to provide senses.

The flexible and stretchable strategies for E-skins are discussed in this review. There are three parts to introduce flexible materials, structural designs, and integration, mainly on

the necessary techniques and achieved developments. This review aims to discover universal methods for fabricating flexible and stretchable E-skins and serves as a basis for further improvements. In Figure 1, we have summarized the framework of this review and listed the contents for each section. In the brief introduction, flexible materials are the foundation of E-skins, including substrates and conductors. Structural designs and integration are necessary steps for the practical applications of E-skins.

In detail, E-skins mimic and function like human skins. Hence, an essential property of E-skins is to satisfy the requirements of flexibility and stretchability. First of all, E-skins are on flexible substrates. E-skins are usually attached to moving and complex surfaces, which undergo stretching, compressing, bending, and twisting. Under these conditions, E-skins need to fit the deformation and adhere to the supporting body and decrease the risk of delamination from the moving surface. In this way, E-skins maintain their functions and sensitivity to environmental variations. From this point, flexibility and stretchability are the properties that need to be considered in the substrate, conducting materials, and structural designs. Recent studies choose polymers as insulated
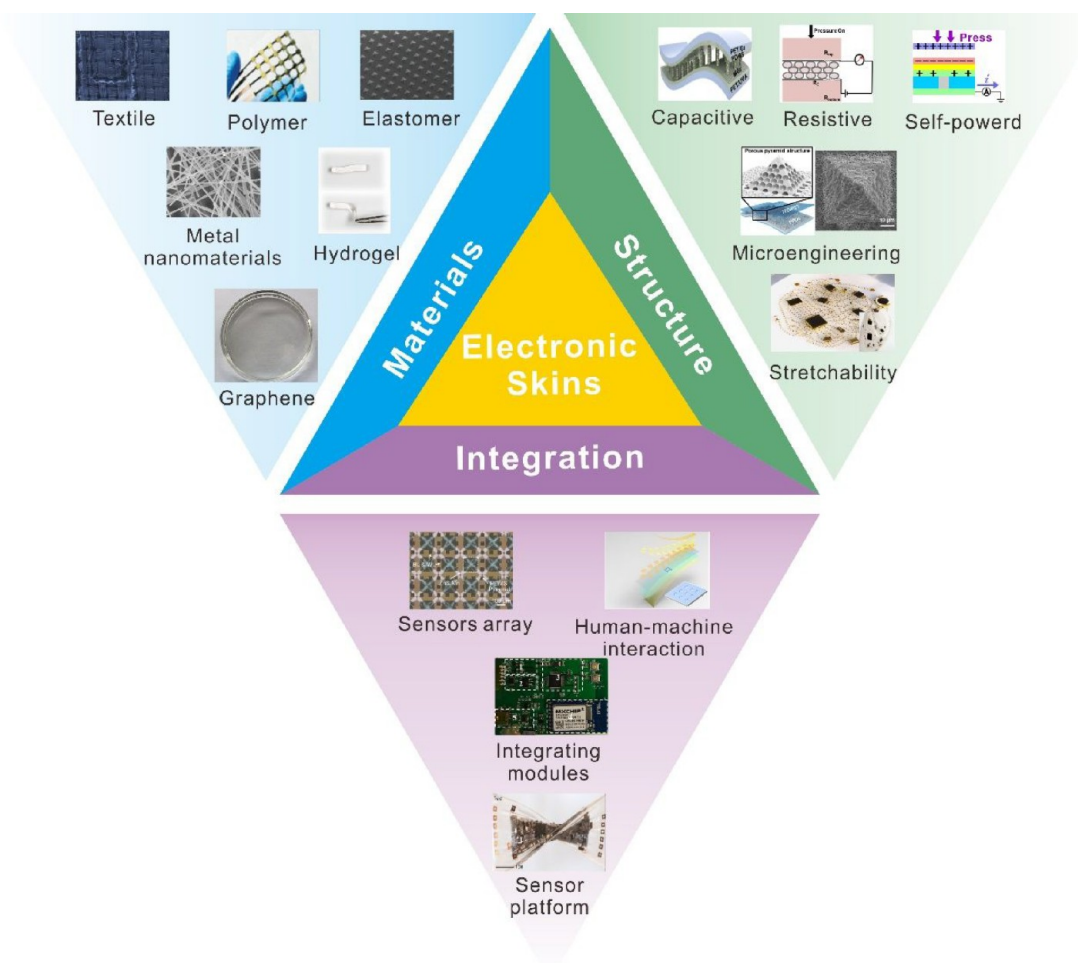
Figure 1. Summary of the review. (i) Flexible materials for E-skins. "Textile", reproduced with permission from ref 25. Copyright 2017, Wiley. "Polymer", reproduced with permission from ref 26. Copyright 2020, Wiley. "Elastomer", reproduced with permission from ref 27. Copyright 2020, Wiley. "Metal nanomaterials", reproduced with permission from ref 28. Copyright 2010, American Chemical Society. "Hydrogel", reproduced with permission from ref 29. Copyright 2019, American Chemical Society. "Graphene", reproduced with permission from ref 30. Copyright 2016, Wiley. (ii) Structure and mechanism for E-skins. "Capacitive", reproduced with permission from ref 31. Copyright 2019, American Chemical Society. "Resistive", reproduced with permission from ref 32. Copyright 2018, Elsevier. "Self-powered", reproduced with permission from ref 33. Copyright 2017, American Chemical Society. "Microengineering", reproduced with permission from ref 34. Copyright 2019, American Chemical Society. "Stretchability", reproduced with permission from ref 35. Copyright 2017, Springer Nature. (iii) Integration and applications of E-skins. "Sensors array", reproduced with permission from ref 36. Copyright 2017, Wiley. "Human−machine interaction", reproduced with permission from ref 37. Copyright 2019, Springer Nature. "Integrating modules", reproduced with permission from ref 38. Copyright 2019, Elsevier. "Sensor platform", reproduced with permission from ref 39. Copyright 2018, Springer Nature.

substrates, which can bear frequent mechanical toughness and microengineering processes. Some polymers can stably support circuits and active parts of the device.[23,24] The conducting materials include metals, carbon-based materials, conductive polymers, and their composites. They constitute conductive pathways with appropriate layouts on the substrate that can connect the functional components. Even the rigid inorganic materials can provide stretchable interconnections for E-skins. By combining a flexible substrate and circuits, E-skins can be structurally or intrinsically stretchable.

Besides stretchability, the working conditions determine the corresponding structure of E-skins. E-skins must obtain complex information from physical variables and fluctuations for robots and prosthetics to handle tasks. Tactile sensing is the most important, such as detecting static pressure, strain, dynamic shear, and slip motion. Resistive, capacitive, and self-powered sensors are introduced in this review for tactile E-skins. We will discuss their differences in sensing mechanisms,

features, geometric designs, and fabrication processes. Moreover, we evaluate the essential parameters, such as the sensitivity, detection limit, linearity, response time, and resolution.

Design and integration toward flexible and stretchable E-skins systems are in the next section. This section reviews the latest research and tries to discover new directions in developing a sensing system. The contents include the sensing array, multifunctional platforms, HMIs, self-powered devices, and integrated modules. Some representative works are emphatically introduced in this section.

In this review, we summarize the flexible and stretchable strategies of E-skins. Section 2 introduces the flexible and stretchable materials and their composites to fabricate E-skins. In section 3, we discuss the sensing mechanisms and structural engineering to establish a tactile E-skin device. An emphasis on how to optimize the parameters of sensors to improve the performance is also in this section. Section 4 introduces recent
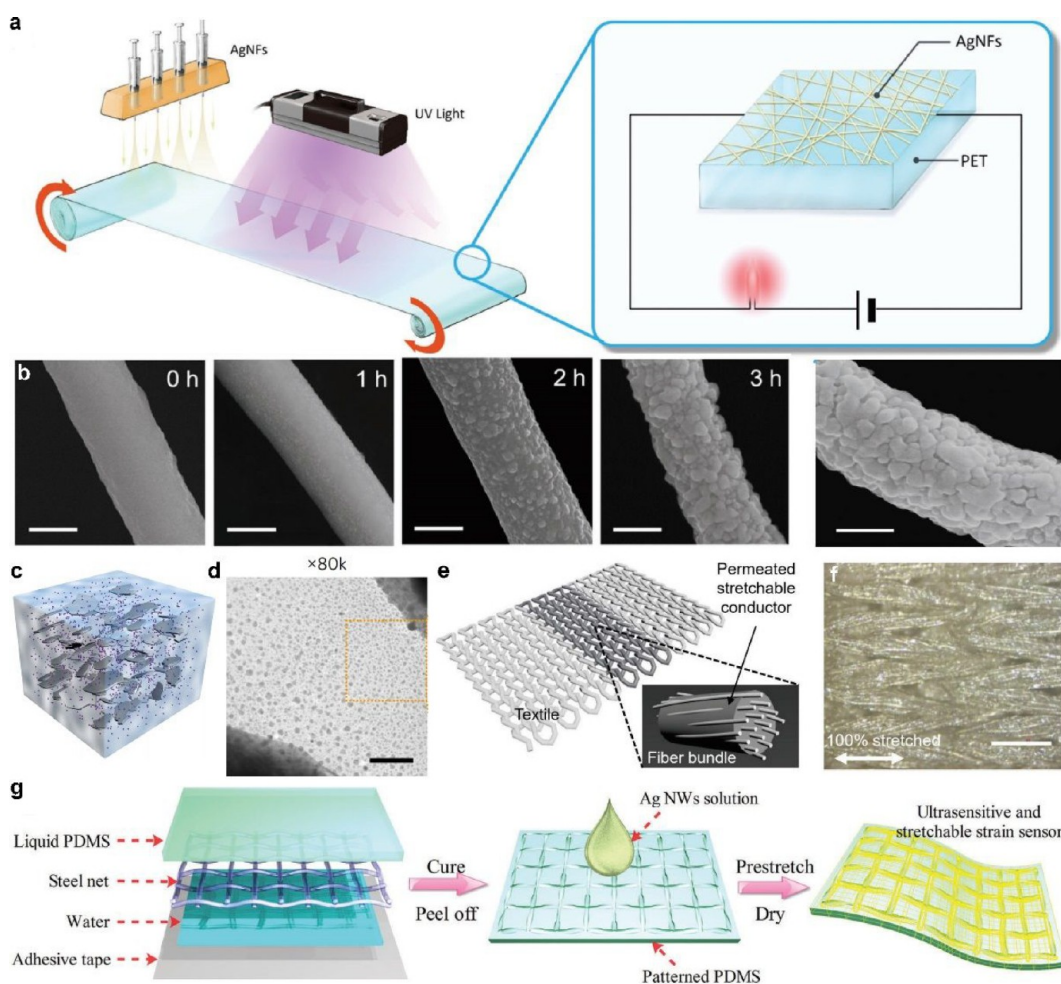
Figure 2. Silver nanomaterials and their devices. (a) Schematic illustration of the UV reduction for silver nanofibers. (b) The corresponding SEM images of the nanofibers covered with silver nanoparticles. Reproduced with permission from ref 72. Copyright 2017, Wiley. (c, d) Schematic illustration (c) and TEM images of silver particles exfoliated from silver flakes (d). Reproduced with permission from ref 84. Copyright 2017, Springer Nature. (e, f) Silver nanoparticles on the conductive and stretchable textiles. Reproduced with permission from ref 64. Copyright 2017, Wiley. (g) Schematic illustration of silver nanowires spreading on the PDMS that was patterned by the steel mold. Reproduced with permission from ref 85. Copyright 2017, Royal Society of Chemistry.

progress in tactile E-skins and focuses on integration and application. The conclusion and perspective are in the final section.

2. FLEXIBLE AND STRETCHABLE MATERIALS AND E-SKINS

There are structurally and intrinsically deformable methods to obtain flexible tactile E-skins. The structurally deformable design is to rationally arrange rigid and active components supported by the flexible substrates. On the other hand, the intrinsically deformable design utilizes flexible and stretchable materials to maintain mechanical and electrical stability under severe deformations. Various materials have participated in the E-skins, which mainly include three categories for substrates and three kinds of conductive materials.

2.1. Flexible and Stretchable Substrates. An essential characteristic of the tactile E-skins is deformable conformability. Unlike silicon and ceramics, E-skins utilize polymers or other flexible materials as the substrate, which overcomes the fragility and satisfies the mechanical requirements. Polyethylene terephthalate (PET), polyethylene (PEN), polyimide (PI), and polycarbonate (PC) are common substrates to fabricate E-skins.[26,33,40,41] These polymer films have superior deformability, mechanical toughness, easy plasticity, excellent insulation, and fitness to most physical, chemical processes. However, these polymers vary in treatment temperature under actual conditions. For PET and PC, the heat temperature should be less than 100 °C without double-sided hardening treatment. PEN can sustain a higher temperature of around 200 °C and possesses excellent transparency. The glass-transition temperature (T_g) of PI is between 360 and 410 °C. Some PI films can even bear a high temperature of 500 °C for a relatively long time to complete the growth of inorganic materials.[42,43] All of the above flexible films can be made into thin electronics to decrease the dislocation from the moving body.

Another type of substrate is intrinsically stretchable material. Polyurethane (PU) has a large elastic modulus. And cross-linked elastomers are more common in this field, especially silicone elastomers, such as commercial polydimethylsiloxane (PDMS, Dow-Corning 184) and silicone rubbers (Ecoflex, Dragonskin, Smooth-on).[44−46] The silicone elastomers take advantage of simple precursors, high stretchability, thermal stability, low toxicity after curing, and easy modification to improve the properties. Benefitting from the adjustable and fluid precursors, silicone elastomers have been made into active structures to enhance the performance of tactile sensors. Some researchers also utilized PDMS to fabricate PDMS-based composites and optoelectronics, which offer the combined properties of light and pressure for E-skins.[47] The silicone elastomers maintain a low elastic modulus to adhere to complex and moving surfaces. They can be used for epidermal electronics.[48] All of the above advantages broaden its applicability as a flexible substrate for E-skins.

Besides the materials described in the previous part, there have been fabric textiles and fiber-based substrates, according to whether they are orderly or randomly fabricated.[49,50] Textile electronics have been developing as a rising type of flexible electronics because they can work as a part of clothes and naturally fit human skins.[51,52] Because of the flexibility and structural stretchability, textiles are close-at-hand substrates for flexible E-skins. In addition to artificial plastics, some researchers seek naturally friendly materials to fabricate E-skins, such as silk and cellulose, to achieve comfort and daily uses.[53,54] Paper is also a low-cost and widely available substrate for E-skins. It is composed of abundant microfibers and is supportable for most flexible conducting materials. With rational manufacturing technologies and tailorable properties, paper is convenient to make desirable shapes, further fabricated as low-cost and sensitive E-skins.[55,56]

2.2. Flexible and Stretchable Conductive Materials.

Human skins provide distinguished functions, such as sensation, mechanical protection, and self-healing. E-skins have stratified and interconnected components compared to human skins, while conducting circuits provide the electrical connections. Flexible conducting materials are essential for the E-skins to possess elongation or compression properties to sustain sensing performance. They need to bear surface moving, pressure loading, substrate bending, and external rubbing. This section summarizes the materials that fabricate conductors and their properties, including nanoscale metals, metal oxides, carbon materials of nanotubes, and graphene, conducting polymers, and hydrogels.

2.2.1. Metallic Nanomaterials: Silver, Gold, and Copper.

Metal is widely used as a conductive material. Conventional inorganic metals in flexible and stretchable electronics usually appear in microscale or nanoscale forms.[57,58] The metal electrodes rely on engineering approaches to achieve structural mechanics and overcome their rigid and brittle properties. Researchers reported that microstructural metallic films could be thin as tens and several hundreds of nanometers in thickness.[59] This nanomembrane is flexible due to the large ratio of bending stiffness scaling with film thickness, compared to bulk metal.

Silver is one of the most conventional conducting metals in flexible electronics due to its high conductance, easy access, and low cost. Silver has a bulk conductivity of 6.3×10^5 S cm^{-1} and is resistant to oxidation at room temperature.[60] Silver-based nanomaterials contain 0D particles,[61] 1D nanofibers,[62] nanowires,[63] and 2D flakes.[64] Silver nanomaterials have been synthesized through chemical and other approaches to control the growth with few defects. Methods of synthesizing silver nanomaterials include polyol approaches, hydrothermal synthesis, electrochemical deposition, and UV-induced reduction.[65,66] In most chemical synthesis methods, $AgNO_3$ is the precursor of the silver source. For instance, in polyol synthesis methods, the reduction of $AgNO_3$ is due to the ethylene glycol (EG), with an appropriate capping agent such as polyvinylpyrrolidone (PVP).

PVP enables the synthesis of silver nanostructures for particles, nanowires, and nanosheets through controlling the temperature, concentration, and other parameters.[67−71] But in the UV-induced reduction method, the reduction can be induced by UV light at relatively low temperatures and even solid-state conditions, as shown in Figure 2a,b.[72] Ligands and additions adjust the methodologies and concentration of silver nanomaterials in chemical reactions. However, they remain as the residual purities.[73,74] So silver composites possess different performances in conductivity as electrodes. Other deposition methods can fabricate silver electrodes, including physical vapor deposition, aerosol spraying, and electroless plating approaches.[75] Silver can be deposited on the substrate with the lift-off process to achieve nanoscale and elaborate patterns according to the designed mask. In fact, despite the enormous progress achieved so far, there are still challenges in producing large-scale metal electrodes with extreme deformability, especially on substrates with different textures and complex curvilinear surfaces. Compared with the rigid substrates, the preparation and working conditions of electrodes on the flexible substrates are complicated. The performance of metal electrodes is more susceptible to substrate strains, which results in stress

concentration, unevenness, and instability. Mainly, it has a bad influence on electronic skins that require high sensitivity and consistency. Therefore, for flexible substrates with nonflat surfaces such as fibers, it is necessary to study the appropriate methods to obtain stable metallic electrodes on the substrates. Even more, nonuniformity with low aspect ratios, highly resistive cross-junctions, and assembly setups are problems that remain to be solved. The challenge in utilizing metallic nanomaterials, such as nanowires and nanoparticles, is that the insulated additions or ligands used for the synthesis and solution dispersion remain with the metallic nanomaterials. These defects decrease the conductivity and introduce mechanical instability for the conductive networks. Various methods have been used to improve the performance, including increasing the aspect ratios of nanowires,[76] optical or heat annealing of the cross-junction,[77,78] utilizing near-field jet printing, and combining with another material.[79] The improvement in the conductive performance of the electrodes will further promote the development of flexible electronics.

Solution-synthesized silver nanomaterials are naturally dispersed and appropriate for conductive inks. There have been many commercially available silver-based conductive inks used for printed electronics.[80−82] However, to achieve a higher conductance and stable connections under large strains, researchers have made contributions to improving the fabrication process.[83] Matsuhisa et al. realized printable silver nanoparticles for flexible electrodes and sensing applications in Figure 2c.[84] They reported an in situ preparation for silver nanoparticles based on a mixed ink comprising fluorine rubber, fluorine surfactant, and Ag micro flakes in the methyl isobutyl ketone (MIBK). The halfway reaction in the process was captured by TEM in Figure 2d, displaying that the nanoparticles mixed with the flakes. The mixed ink was printable for fabricating conductive routines after drying and heating. Moreover, the optimal process of forming nanoparticles has been made to improve the conductivity under strains. The stretchable conductive lines displayed up to 4900 S cm^{-1} in the original length and 700 S cm^{-1} with 300% elongation. The authors also fabricated stretchable pressure and temperature sensors by printing, with the silver interconnections to demonstrate the performance. The results show that the sensors remained functional at a strain of 120%.

Silver nanowires and PDMS substrates often appear in pairs for fabricating stretchable strain sensors. The conductive network of silver nanowires deforms with the elongation and compression of PDMS. Liao et al. exhibited a microcrack strain sensor which achieved a tremendous gauge factor (GF) of 150 000 within 60% strain.[85] The authors utilized a steel net to fabricate uniform micropatterns on the PDMS substrate in the experiment, as shown in Figure 2g. The steel mold provided controllable channels for conductive ink of silver nanowires to spread, which could rapidly establish conductive channels. With the help of prestretching, the silver nanowires filled the microcracks and surface of stretched PDMS. The results showed that the microcracks of conductors expanded to maintain the connections under stretching. The micropatterned PDMS remained a lower resistance than that of flat PDMS under 60% elongation while achieving a much higher sensitivity. Furthermore, the strain sensor displayed a fast response and excellent stability.

Silver flakes were also used for conductive electrodes. They can be attached to the textile substrates for detecting human biomechanical signals. Jin et al. reported a conductive knitted fabric infiltrated by silver flakes ink in Figure 2e.[64] The ink consisted of P(VDF-HFP), 2-(2-butoxyethoxy) ethyl acetate, and silver flakes in a weight ratio of 1:2.45:4. Then the silver flakes ink was printed on the textile repeatedly to confirm that the solution was absorbed into the interior of the fabric, followed by drying and hot-press treatment. The images in Figure 2f demonstrated that the silver flakes filled the surfaces and small gaps of the knitted fabrics, which realized complete conductive pathways along the fibers. The conductive fabric sheet resistance was 0.06 Ω sq^{-1} at the initial stage and only increased by about 70 times after 450% stretching. The conductive fabric lit a LED under the strain of 400% and maintained its performance. The authors built an
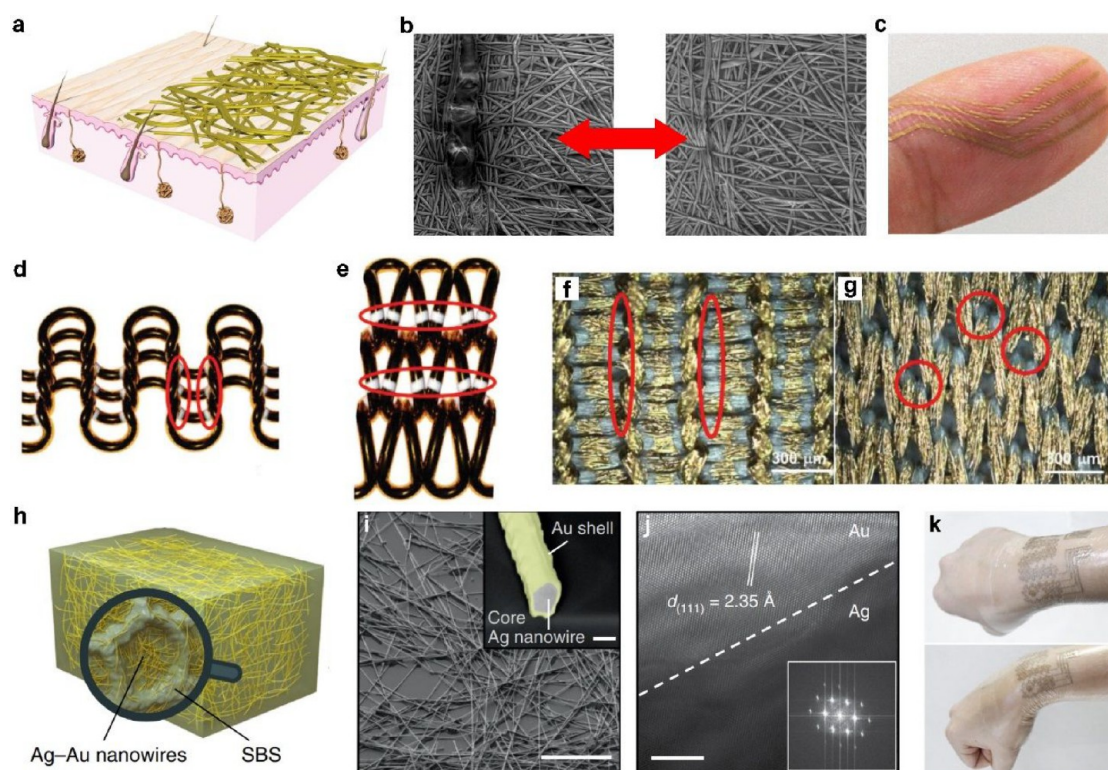
Figure 3. Gold nanomaterials and their devices. (a) Schematic image of the gold nanomesh conductor. (b) SEM images of the nanomesh during and after strain. (c) The photo of nanomesh on the finger. Reproduced with permission from ref 92. Copyright 2017, Springer Nature. (d, e) Illustrations of stretchable textiles in the course (d) and wale directions (e). Optical images of stretched gold textiles in the course (f) and wale directions (g). Reproduced with permission from ref 93. Copyright 2018, Wiley. (h) Schematic image of the gold-coated silver nanowires in SBS. (i, j) SEM and TEM images of the nanowires. (k) Photo of conducting circuits based on the composites of conductive nanowires and SBS. Reproduced with permission from ref 94. Copyright 2018, Springer Nature.

electromyography (EMG) monitoring system based on this printed textile circuit to sense the muscle motions and corresponding signals.

Similar to silver, gold nanomaterials include 0D nanoparticles, 1D nanowires/rods/belts, and 2D flakes/sheets.[86] Gold is a widely used conductive material due to its corrosion resistance and excellent bulk conductance ($\sigma = 4.10 \times 10^5$ S cm^{-1}). It was stable in many chemical conditions and resistant to oxidization at high temperatures. Gold nanoparticles can be from reducing chloroauric acid (H[AuCl]$_4$) in a solution. The reducing agents are generally citrate, tannic acid, sodium borohydride, and hydroquinone. Moreover, oleylamine could be a stabilizer when synthesizing gold nanowires in a similar chemical method.[87,88] Gold nanoflakes could be obtained through controlling the reaction environments and parameters.[89−91] Other physical means are also accessible to synthesize the gold nanoparticles, such as PVD and ELD processes.

Highly stretchable and ultrathin gold nanomesh based on the nanofibers was used to achieve air-permeable and lightweight E-skins. Miyamoto et al. reported a method of fabricating gold nanomesh by sacrificing poly(vinyl alcohol) (PVA) nanofibers in Figure 3a−c.[92] The experiment deposited 85 nm gold film on the PVA nanofibers through thermal deposition, followed by dissolving the PVA nanofibers with spraying water. In this way, the gold nanomesh could attach to the human skin for a period, leaving a conductive electrode for E-skins. The diameters of PVA were around 300−500 nm, which mold the shape of gold nanomesh. The SEM images in Figure 3b show that the nanomesh was attached and fit the ridges on the fingertip. So as thin as the nanomesh was, the conductive stripe could open voids under the strains of skins. The authors tested the conductance of the gold nanomesh under different stretchable deformations. The initial conductance was 2.9×10^{-3} S. Then, an elongation of 40% decreased the conductance to 7.1×10^{-4} S. Repeated test of stretching showed that the conductance was reversible. The authors used the gold nanomesh to fabricate touch,

pressure, and temperature sensors for the on-skin wireless systems to demonstrate the conductivity. The results showed that the conductance of the nanomesh stripes changed with pressure and temperature, which achieved an excellent response to external stimulations.

General conductive inks mix with a binder to guarantee attachment on the substrates. But some types of binders are hard or brittle after curing, which might be harmful to the flexibility. For instance, the ink possibly permeates the gaps and voids in the knitted fabric to rigidify the structure. Wu et al. uniformly covered the fibers with gold particles, leaving enough space for the movements.[93] In the experiment, electroless nickel immersion gold (ENIG) was used for the core−shell fabric, as shown in Figure 3d,e. This method coated the fibers with Ni and Au in sequence to obtain a low sheet resistance of 1.07 and 3.33 Ω sq^{-1} in the course and wale directions. Figure 3f,g shows the optical images of the fiber architecture, where there was an approximately 80 nm gold layer outside the fiber. The fabric was used to assemble an electroluminescent device. The fabricated device gave out blue and uniform emission with increasing strains, demonstrating the stable conductance of the fibers.

Combining the properties of silver and gold can achieve an enhancement in conductivity. Kim et al. synthesized gold-coated silver nanowires in Figure 3h.[94] As-fabricated silver nanowires were as long as 100 μm. The SEM and TEM images of the nanowires are shown in Figure 3i,j. The shell layer of gold was *in situ* formed on the silver nanowires through the reduction of HAuCl$_4$. After mixing Au@ AgNWs with the SBS precursor in an appreciated proportion, the mixture was cured to obtain conductive elastomer composites. The composite (60:40 in weight) retained a conductance of 10^4 S cm^{-1} under an elongation of 150%. However, the high concentration of nanowires might reduce the stretchability. Because of the fluid mixtures, the composites were easily cast into patterns and assembled into conducting circuits for a multifunctional E-skin device, as shown
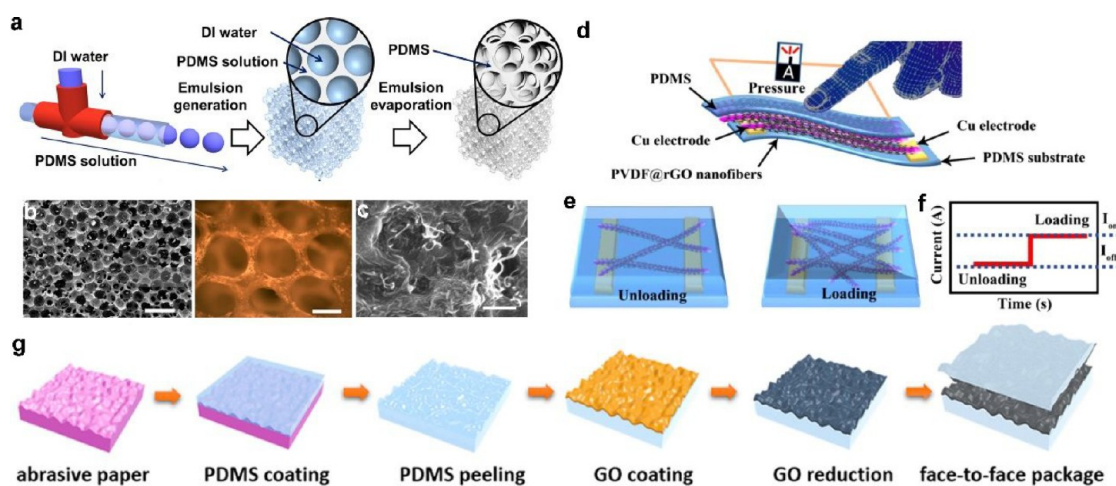
Figure 4. Carbon-based nanomaterials and their devices. (a) Schematic illustration of fabricating porous PDMS. (b) The SEM and optical images of the porous PDMS. (c) The composite of CNTs and porous PDMS. Reproduced with permission from ref 113. Copyright 2019, American Chemical Society. (d−f) The working schematic of the PVDF@rGO-based pressure sensor. Reproduced with permission from ref 141. Copyright 2016, Elsevier. (g) The schematic illustration of fabricating the pressure sensor with interlocking rGO/PDMS films. Reproduced with permission from ref 142. Copyright 2018, American Chemical Society.

in Figure 3k. The conductive composites could measure electrophysiological signals and support electrical and thermal stimulations under strains.

Different from the precious metals of silver and gold, copper is abundant in the natural environment and has more potential in commercial applications. Copper reserves may be 1000 times that of silver. Copper nanomaterials might benefit from the cost to fabricate flexible and stretchable conductive circuits in the E-skins. Using nanowires has been one of the most convenient choices to build flexible electronics based on copper nanostructures.[95,96] Copper nanowires were synthesized by solution methods such as the reduction method.[74,97,98] And additions such as hydroxypropyl cellulose to the solution will improve the homogeneous and well-dispersed properties.[99] However, copper nanomaterials are susceptible to oxidization without proper protection. Cu nanomaterials easily react with oxygen under air-ambient conditions and become nonconductive. Moreover, increasing the temperature can accelerate oxidization. So the protection of Cu nanomaterials from corrosion has been essential for conductive performance. Coating with conductive oxides, Zn, Ni, and graphene as the passivation layer could be an effective solution.[100−103]

2.2.2. Carbon Nanotubes (CNTs) and Graphene. One-dimensional nanotubes and 2D graphene have been widely studied to realize flexible and stretchable E-skins. CNTs include two kinds of single-walled CNTs (SWCNTs) and multiwalled CNTs (MWCNTs), and three armchair, zigzag, and chiral structural forms. They are semiconductive or metallic due to the chirality of CNTs. Recent research has explored the solutions of achieving a large aspect ratio, dispersing in polar solvents, decreasing defects in the carbon walls, and purifying. Moreover, researchers have developed laser ablation, arc discharge, and chemical vapor deposition (CVD) methods to synthesize large-area and low-cost CNTs.[104−106] Nowadays, the length of CNTs could reach half a meter by controlling CVD growth parameters.[107] And the same group's further work retained the level of centimeters and displayed ultrahigh fatigue resistance by decreasing the defects.[108] The improvements achieved in chirality control, purification, and functionalization enhance the properties and expand the potential applications of CNTs. For E-skins, high-aspect-ratio CNTs can establish highly stretchable and conductive networks. They can be assembled on or into the elastomer substrate to provide the conductive pathways under large deformation.[109,110] Also, CNTs electrodes can be directly deposited onto the flexible substrates by solution spraying, spinning coating, ink-printing, and vacuum filtration.[111,112] And CNTs can be distributed locally as channels of

thin-film transistors (TFTs) for stretchable E-skins to fit complex and deformable tactile conditions.

Some other research focused on utilizing CNTs to fabricate 3D conductive patterns or networks. CNTs were mixed with PDMS precursors. Then the mixture was cast on a micropatterned silicon mold to form a conductive and pressure-sensitive composite. There were many microdomes on the surface of the cured composite film, which enlarged the strains under vertical pressure. The pressure sensor can achieve a high sensitivity of 15 kPa^{-1} in the vertical direction by interlocking two micropatterned composite films. Similar to microdome composite films, a porous CNTs/PDMS composite was also used for sensing tactile pressure. Porous structures were more deformable than the compact bulks because only thin walls between the pores could share the internal stress. The voids in the structure decreased the compressive modulus of the overall structure and increased the strains under pressure. Kim et al. fabricated porous CNTs/PDMS composite films as the resistive pressure sensors in Figure 4a−c. The applied pressure significantly changed the conductivity to realize high tactile sensing sensitivity.[113] Capacitive sensing was also achieved based on porous CNTs/PDMS composites.[112] Moreover, CNTs in the composite film could repair mechanical damages. Dynamic reconstruction of a conducting network showed that the reorganization of CNTs contributed to the self-healing process of polymers and finally recovered the conductance and mechanical properties of the flexible film.[114]

Graphene has been coupled with elastomers to fabricate flexible and stretchable sensors. It has many characteristics, such as excellent mechanical properties, high transport carrier mobility, and optical transparency.[115] Usually, graphene is divided into four kinds of graphene sheets (GS), graphene ribbons (GR), graphene oxide (GO), and reduced graphene oxide (rGO). They are determined according to the surface modification and geometric structure of the materials.[116−119] Among them, GS and rGO possess superior conductivity than the others, which are more common in flexible electronics as physical sensors.

There have been developments of two fabricating top-down and bottom-up approaches for graphene.[120] The top-down approach is exfoliating graphene from graphite and CNT with mechanical, solution, and chemical ways. These techniques are probably low-cost and large scale. However, they produce a large ratio of carbon flakes in the process and decrease graphene purity. Moreover, quantitative defects remain in the graphene sheets. The bottom-up approach assembles carbon atoms into graphene through CVD, epitaxial growth, and organic synthesis. Compared to the top-down approach, the bottom-up approach can produce graphene with higher
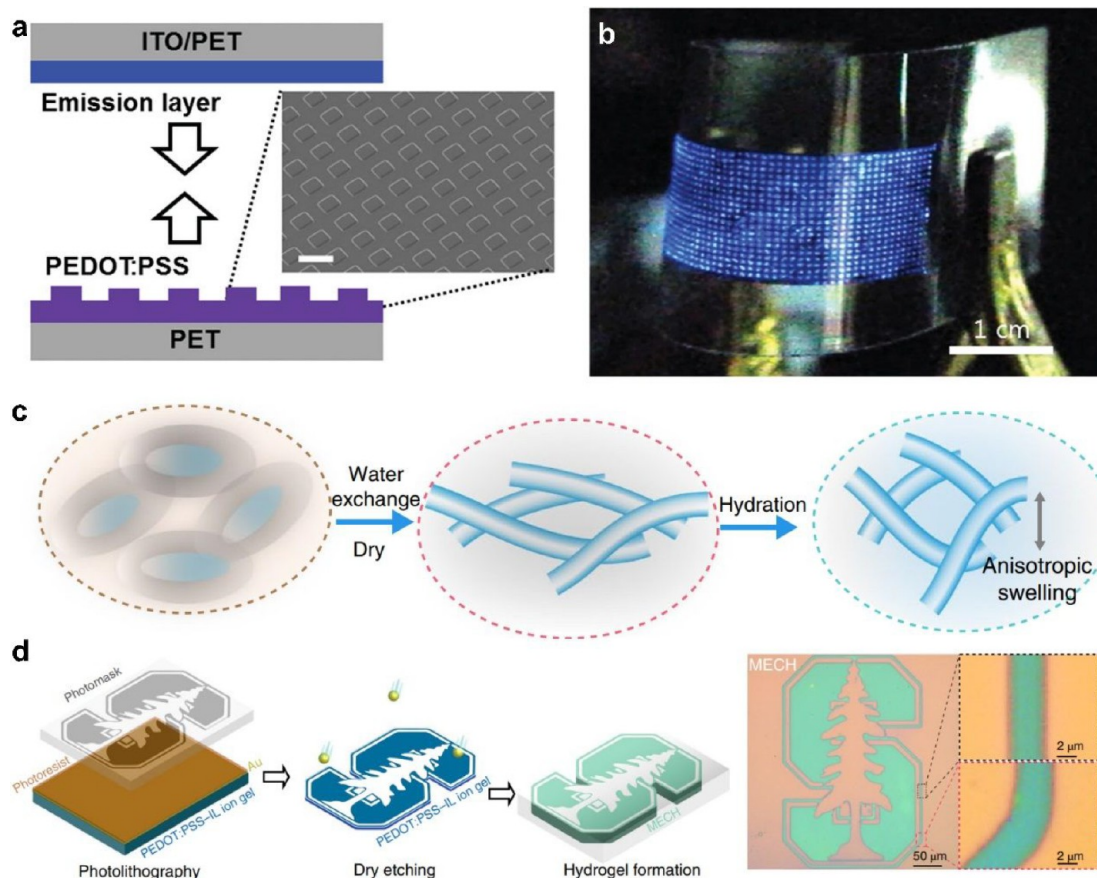
Figure 5. Conductive polymers. (a, b) Schematic illustration and image of the square PEDOT:PSS patterns for OLEDs. Reproduced with permission from ref 147. Copyright 2016, Wiley. (c) Schematic of the stepwise synthesis process for PEDOT:PSS electrically conductive hydrogels by blending, water exchange, drying, and swelling to form the conductive pathways. (d) Schematic illustration of lithography for the hydrogels. Reproduced with permission from ref 148. Copyright 2019, Springer Nature.

purity and fewer defects. However, its expensive cost limits potential applications in large-scale production.

After synthesizing graphene, establishing a macroscopic and conductive electrode is essential for E-skins. There have been several approaches to assemble flexible and stretchable graphene devices so far, such as the template method, self-assembly method, coating method, and 2D and 3D printing method. The coating and 2D printing methods are carried out similarly to metal nanomaterials and CNTs in the previous sections. Graphene can be dispersed in inks and utilized to form conductive films by dipping, spinning, spraying, and printing approaches.[121−124] The graphene ink is patterned into specific routines by masks and solidified to assemble conductive electrodes. 3D printing techniques have been used for the intelligent manufacturing of graphene 3D architectures, which model the graphene solution or mixture into a solidified structure in a precise and rapid process. For example, thermoplastic filaments mixed with graphene can be melt and extruded to print the desired architecture layer by layer. The graphene ink with a very high viscosity can be extruded from the printer tip and cured by heat simultaneously on the substrate.[125,126] The laser is also used for the graphene electrodes. Compared to the direct writing, a high-energy laser beam is pulsed to sinter the composite powders with a graphene source and catalyst. Moreover, the laser can also accelerate the curing of the photosensitive resin that contained graphene with high resolution.[127,128]

Another approach is mixing graphene into elastomers to obtain flexible and stretchable conductive composites. The process can achieve a uniform and conductive polymer film by infiltrating the graphene sheets with elastomer precursors, defoaming, and drying or heat preserving.[129] Most substrate materials are described in the previous section, such as PDMS, Ecoflex, and PU. Some other polymers can also provide a supporting framework for the conductive films without stretchability, such as PI.[130] Various mass production techniques have been utilized to manufacture flexible graphene/polymer composites, including in situ polymerization, solution blending, and melt compounding.[131] Furthermore, graphene can be assembled by various types of templates. These templates provide support and space for graphene, and graphene fills the spacer and gathers to form conductive routines due to the excellent adsorbability.[132−135] Moreover, supramolecular interactions of π−π bonding, hydrogen, and electrostatic interactions are possible approaches to produce self-assembly structures.[136,137]

Graphene with high electrical conductivity and flexibility has many applications in E-skins. One of the emerging applications is the resistive pressure sensor. Pressure-sensitive structures include the micropatterns of pillars, bubbles, and honeycombs as the active parts in the flexible pressure sensors.[138−140] Lou et al. used rGO-coated P(VDF-TrFE) nanofibers to fabricate conductive networks in Figure 4d.[141] The vertical compressive pressure on the nanofiber film changed the nanogaps between the conducting pathways, as shown in Figure 4e−f. In the applications of sensors, graphene counted on the flake size, contact resistance, and surface treatment or modification to improve the conductive performance, which further enhanced the sensitivity of the whole structure for pressure. Moreover, the dispersion of graphene in the matrix could change the tunneling resistance between the successive graphene sheets and influenced the sensing properties. Pang et al. developed a method to fabricate a microstructured pressure sensor with interlocking rGO/PDMS films in Figure 4g.[142] This sensor worked as a wearable health monitor, which could detect wrist pulse, respiration motion of the chest, and other biomechanical motions. Because of the properties of rGO and
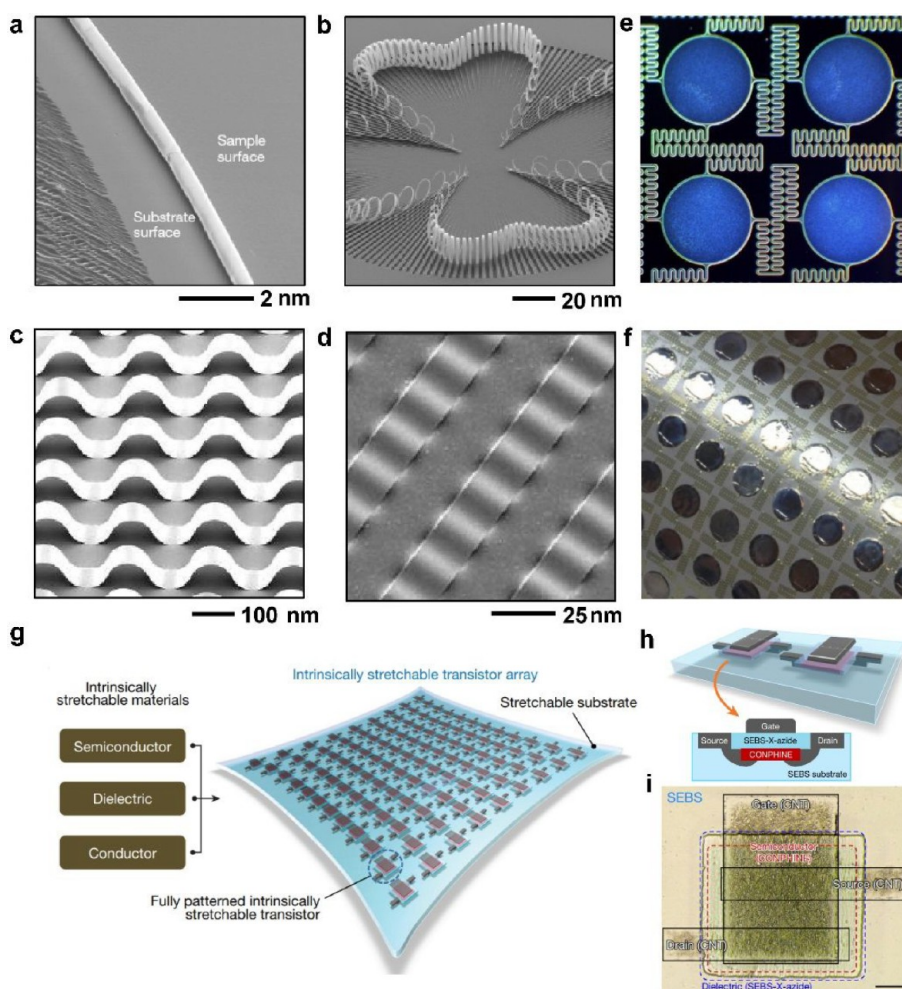
Figure 6. Structurally and intrinsically stretchable designs. (a−d) SEM images of structurally stretchable semiconductor nanomembranes, nanotubes (a), coil structures (b), buckled ribbons (c), and wavy ribbons (d). Reproduced with permission from ref 163. Copyright 2009, American Chemical Society. (e, f) Fractal-inspired interconnect designs on a Si wafer (e) and transferred onto the silicone (f). Reproduced with permission from ref 188. Copyright 2013, Springer Nature. (g) Schematic diagram of an intrinsically stretchable transistor array. (h, i) Schematic illustration and photo of an intrinsically stretchable transistor. Reproduced with permission from ref 187. Copyright 2018, Springer Nature.

microstructures, the sensor realized a wide linearity range of 0−2.6 kPa and a high sensitivity of 25.1 kPa^{-1}.

2.2.3. Conductive Polymers and Hydrogels. Conductive polymers of poly(3,4-ethylene dioxythiophene) (PEDOT), polypyrrole (PPy), and polyaniline (PANI) have been widely studied due to their mechanical properties, easy modification, and conductivity. The conductivity is from the delocalized electrons or holes in the conjugated backbones of the structure. However, to satisfy the requirements of the flexible electrodes and active layers of E-skins, these polymers are usually incorporated with ionic electrolytes to introduce more dopants for charge transportation. PEDOT:PSS has been commercially available among the doped polymers and has attracted extensive attention, which is from PEDOT doping with poly(styrenesulfonate) (PSS). PEDOT:PSS is a heavily p-doped organic conductor. Its electrical conductivity can exceed 1000 S cm^{-1} and can be for conductive solutions or inks. The high conductivity of PEDOT:PSS usually comes from two pathways in the polymeric matrix. One is the electronic carriers along the polymer chains. The other is the ionic soft polymer matrix with sufficient hydration in water.[143,144] However, the GPa-scale Young's modulus makes it difficult for PEDOT:PSS to fabricate stretchable electronics. Only a 5% strain would induce ruptures in the stiff matrix.[145] To improve the stretchability, PEDOT:PSS can be blended with plastic additives to enhance the deformability. Wang et al. incorporated ionic liquids into PEDOT:PSS to enhance both stretchability and electrical con-

ductance.[146] The fabricated PEDOT:PSS film could realize a maximum strain of 800% before the substrate fractured and retained a conductance of 4100 S cm^{-1} under 100% strain. The improvement in conductance was due to the addition of ionic liquid. The ionic liquid weakened the electrostatic effect between the PEDOT and PSS. It transformed the whole structure to two isolated parts in the mechanical properties. The PSS part with fluidity could expand with the substrate and enlarge the stretchability. In contrast, the PEDOT part kept its rigid properties in the fluid PSS. In this structure, both PEDOT and PSS contributed to the conductance and worked independently under strain.

Oh et al. obtained a viscoelastic PEDOT:PSS rubber with a nonionic surfactant of Triton X-100.[147] Only 0.7% additive Triton X-100 achieved a maximum rupture strain of around 60% for PEDOT:PSS. The square-patterned PEDOT:PSS could support the OLEDs in Figure 5a,b. Another work of Liu et al. overcame the cytotoxicity caused by fluorosurfactants and ionic liquids.[148] The hydrogel replaced ionic liquid to obtain PEDOT:PSS, with aqueous stability, biocompatibility, and partial loss of electrical conductivity and stretchability. Therefore, the feature of combining electrical and ionic conductive pathways enlarged the applications of PEDOT:PSS. This feature also enables the PEDOT:PSS as the active channel to fabricate organic electrochemical transistors (OECTs).[149,150] The PEDOT:PSS in the OECTs is exposed to an electrolyte or ionic fluid

to detect chemical substances, which has essential biological sensing applications.

Ionic hydrogels are based on a polymer matrix to provide mechanical support. Water makes up the rest weight as high as 90%.[151] They are very similar to biological tissues in mechanical performance, chemical properties, and ionic transportation.[152] So hydrogels are suitable candidates for epidermis electronics and E-skins applications. The forming approaches of the hydrogel matrix include chemical cross-linking, ionotropic cross-linking, and electrostatic interactions. And the polymer network included polyethylene glycol (PEG), polyacrylamide (PAA), poly(vinyl alcohol)(PVA), and their copolymers.[153−155] The Young's modulus of these hydrogels was usually at the level of Pa or kPa, which made the materials soft and increased the convenience to attach to the epidermis or other complex surfaces. Some researchers also obtained dense and robust hydrogels with the Young's modulus of several MPas.[156,157] The ionic conductivity of the hydrogel could be tuned from 10^{-5} to 10^{-3} S cm^{-1}. So the chemical modification could adjust the properties of hydrogels for various applications.

Ionic hydrogels are motivated by applications in biology. The biocompatibility and softness made it possible for ionic hydrogels to simulate biological tissues. For example, hydrogels can achieve capacitive coupling at the interface or electric double layer (EDL) between the metal electrode and hydrogel, which transfers the electric pulses into the ionic current. The smooth drop in voltage at the interface could effectively decrease the risk of local heating, degradation, and immunochemical reactions. And the hydrogel can be used as a buffer layer to slow down the action potentials, which supports high-frequency stimulation.[158]

In the other aspect, the researchers have studied electronic hydrogels to improve electronic conductivity and performance. The primary method of electronic hydrogels is to incorporate electrically conductive fillers such as conductive polymers. The ionic conductive pathways are substituted by electrically conductive polymers or combined to achieve a compound mode.[159] In these situations, the hydrogel networks provide mechanical properties. Various approaches that include water exchange, infiltration of secondary polymer, in situ polymerization, and electrochemical deposition have been developed for fabricating electrical hydrogels.[148,160,161] As commercially available conductive polymers, PEDOT and PEDOT:PSS have raised attention in the electronic hydrogels. Feig et al. fabricated a loosely cross-linked PEDOT:PSS network infiltrated by a PAA-based secondary polymer skeleton.[160] The result achieved a high conductivity of 0.23 S cm^{-1}. The secondary polymer network could control the Young's modulus of the whole hydrogel due to the low concentration of PEDOT:PSS and retained the conductivity and stretchability at the same time. Microengineering for hydrogel is a possible method for further applications in flexible electronics. Liu et al. developed a method of fabricating hydrogel patterns at a feature resolution of 5 μm through photolithography.[148] In the experiment, an ion gel of PEDOT:PSS was patterned through photolithography and dry etching as the hydrogel precursor. Then the precursor transformed the micropatterns into a conductive hydrogel by water exchange, as shown in Figure 5c,d. The fabricated patterns were conductively stable and tolerant to mechanical strains.

3. TACTILE SENSING MECHANISMS AND STRUCTURES OF E-SKINS

3.1. Flexible and Stretchable Architecture and Materials.
3.1.1. Structurally Stretchable Designs for Inorganic Materials. The natural rigidity and brittle characteristics of inorganic materials limit their applications in stretchable electronics. But rational mechanical designs and strategic integrations enhance the stretchability of inorganic materials and retain the intrinsic properties of high electric performance at the same time.[162,163] Stretchable inorganic electronics have broadened conventional electronic applications and covered an active field in flexible elec-

tronics.[13,164−166] In general, stretchable inorganic electronics include conductive composites, liquid metals, and structural conductors.[167] But only structurally designed conductors are deformable along with the substrates. The structural designs include the wavy, island-bridge, fractal, and kirigami designs, as shown in Figure 6a−f. The thin inorganic materials are embedded to elastomer substrates and achieve a high level of deformation and stretchability on the scale of nanometers.[94,168,169]

In the wavy design, the extremely thin silicon with a thickness down to nanometers meets the large stretchability. Thin inorganic materials like silicon ribbons were transferred onto the prestretching elastomers and formed strong bonding with the substrate. After releasing the stress, the tensile strain transformed into the amplitudes and wavelengths of the wavy structure.[170,171] Beyond the wavy designs, the island-bridge structure comprised rigid functional components and stretchable electrical interconnections.[172,173] The rigid parts were the strongly bonded islands, and the conductive interconnections were the weakly bonded bridges. On the basis of this design, the strains were mainly accommodated by stretchable bridges. The bridges further are divided into four classes of the arc-shaped, serpentine, 2D spiral, and 3D helical designs according to the structures of interconnections.[174−178] Another fractal design achieves high areal coverage for stretchable inorganic electronics. The fractal interconnections fill the 2D plane with repeated stretchable structures in the fractal orders. The bonding process can refer to wavy and island-bridge design. However, the 2D fractal structure might deform out of the plane according to the assembly process.[179,180] Kirigami design for stretchable electronics is based on cutting and folding techniques, consisting of periodic and ordered cutting. This structure realizes planar stretching by expanding the fold ribbons, and the kirigami sheets share the deformable strains uniformly. Kirigami design retains conductivity with enhanced tolerance to tearing force.[181,182]

3.1.2. Structural Designs for Intrinsically Stretchable Materials. Intrinsically stretchable organic materials with high durability, mechanical stability, convenience, and low-cost fabrication also provide stretchability for E-skin devices. Although exhibiting some drawbacks compared to metal and other materials, researchers have made improvements. For example, stretchable transistors are used for E-skin applications.[183,184] The channels can be made up of P3HT, CNTs, and some other organic materials, and CNTs can also work as electrodes. The stretchable semiconductors and electrodes contribute to the fabrication of stretchable transistors, which can work with a mobility of $10^{-2}-10^{-1}$ cm^2 V^{-1} s^{-1} under over 100% tensile strain. The ion gels can substitute the gate electrode and dielectric in the stretchable transistors. Some results showed that mobility was as high as 10 cm^2 V^{-1} s^{-1}.[185,186] Wang et al. fabricated a matrix array of intrinsically stretchable transistors with high uniformity, which work as active-sensing E-skin devices in Figure 6g−i.[187] The substrate, semiconductor, dielectric, and conductor materials utilized in the experiment were stretchable, and the whole E-skin adapted to the shape of the human hand.

3.2. Mechanisms and Structural Designs of Pressure, Strain, and Self-Powered Sensors.
3.2.1. Resistive Pressure Sensing and Structural Designs. Resistive pressure sensors transfer applied pressure into electrical resistance. The following equation expresses the electrical resistance.
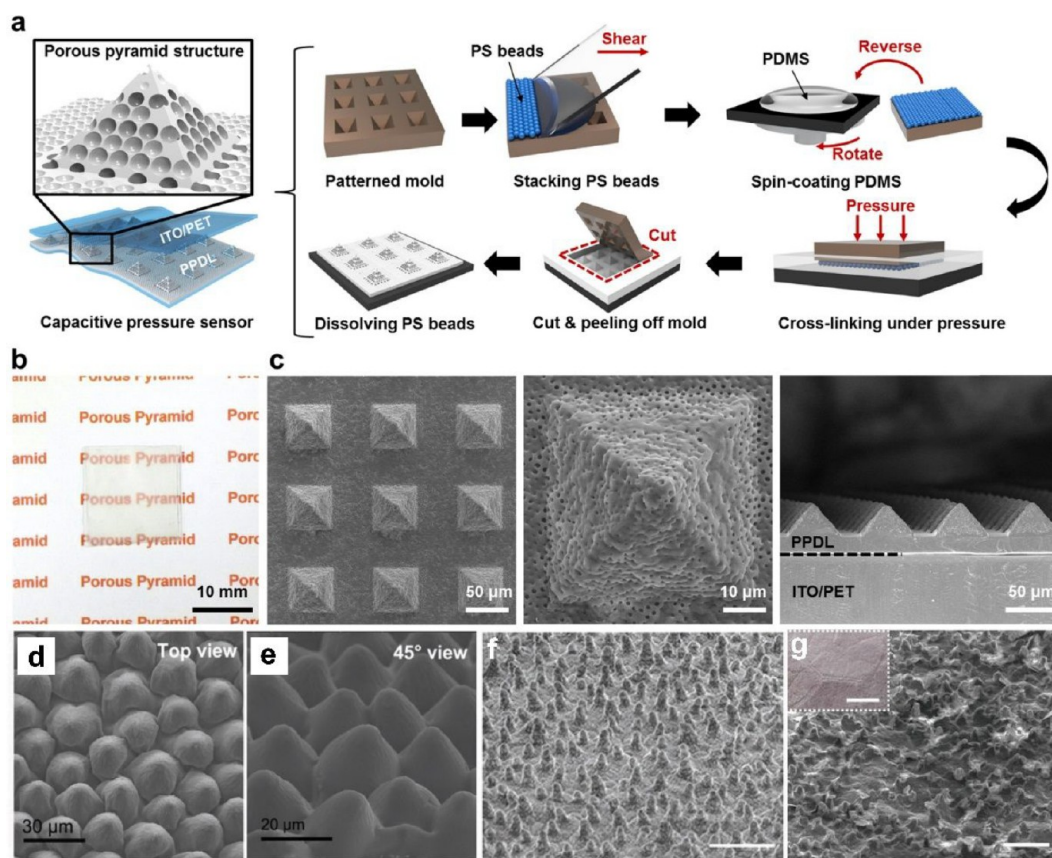
Figure 7. Microengineering approaches. (a) Schematic illustration of fabricating a porous pyramid structure for the capacitive pressure sensor, including blending, molding, curing, and dissolving the sacrificial materials. (b) Optical photo of the porous pyramid dielectric layer. (c) SEM images from the top and cross-sectional view of the pyramids. Reproduced with permission from ref 198. Copyright 2019, American Chemical Society. (d, e) SEM images of the petal-patterned PDMS film. Reproduced with permission from ref 201. Copyright 2015, Royal Society of Chemistry. (f, g) SEM images of a lotus leaf (f) and a patterned graphene/PDMS (g). Reproduced with permission from ref 197. Copyright 2018, Wiley.

$$R = \frac{\rho L}{A} \tag{1}$$

In the equation, R, ρ, L, and A are contact resistance, material resistivity, length, and contact area. The applied stress will induce a relative change of the active layer in conductive pathways and further decrease the contact resistance of the device. Usually, the relative change in resistance is given by $\Delta R/R$ to describe the relationship between resistance and pressure. The resistive pressure sensors are supported by a constant supply to achieve durable detection, so power consumption generates Joule heat and impacts the device temperature during working.[189] To overcome the limitations of modulus, viscoelasticity, and thermal stress, there have been many reports covering materials and structural designs to enhance the sensing performance. Microengineering is one of the efficient approaches to adjust the mechanical properties of the active layers to improve the performance of the sensor, including micropatterns, micropores, and multilayers.[190−193]

Micropatterns in the pressure sensors introduce air spacers in the resistance-active layer between the top and bottom layers, which can deform more easily than the flat films. The micropatterns are precisely designed pyramids, microdomes, and semicylinders by controlling the size and distribution.[194,195] The properties of these patterns are different in their mechanical properties, so the pressure sensors feature the performance according to the practical situations. The stress

distribution on the top tip of the pyramid structure is nonuniform.[196] There is a small initial value of the sensing, and it generates an apparent change of resistance under a relatively small pressure. Microdomes and transverse semi-cylinders possess a more uniform change in the contact area to maintain the sensitivity at a given pressure. Also, the hierarchical structure that comprised nanodomes on the hemisphere was fabricated by Shi et al. to realize a more stable and sensitive response.[197] The pressure sensor with the hierarchical structure displayed a higher sensitivity and sensing range.

Porous design is a practical approach to improve the performance of resistive pressure sensors. The size and density of micropores can change Young's modulus of the active layer, which directly affects the sensitivity of the sensor.[198,199] The compressive stress determines the changes in the effective contact area. So the active layer is more deformable due to the larger pores and porosity with higher sensitivity but decreasing the range for detection. Furthermore, the porous structures are divided by whether the pores are open to external environments. The pores have enclosed walls and can bear great weight.

The multilayered stack structure can also be used to fabricate the active layer.[200] The sensor works based on the interactions among the stacks themselves to improve the sensitivity. For example, PDMS microspheres were wrapped by

CNTs and stacked as the active layer. The active layer and the interactions among the spheres contributed to the resistance change under pressure.[193] Wei et al. demonstrated the concentrated stress at the contact points and further discovered the multilayer working mechanism for the resistive pressure sensor.[201]

3.2.2. Capacitive Pressure Sensing and Structural Designs. The prototype of the parallel-plate capacitive sensor inserts a dielectric layer between the top and bottom electrodes. The applied pressure mainly changes the distance between the two electrodes to induce corresponding capacitive changes, which an equation can describe:

$$C = \frac{\varepsilon_r \varepsilon_0 A}{d} \tag{2}$$

C is the sensor capacitance, ε_0 is the vacuum permittivity, ε_r is the relative permittivity of the dielectric, A is the overlapping area, and d is the distance between the two electrodes. Several aspects enhance the performance of capacitive sensors, including the materials and geometric structure, which contribute to the stretchability, linearity, and response time of the whole device. Compressive modulus and dielectric permittivity are essential factors to improve capacitive sensing.[202] The dielectric permittivity determines the capacitance before and during sensing. The modulus might influence the deformable strains and recovery time of the dielectric materials under the same pressure.

By introducing a second substance, such as air voids, the dielectric layer becomes a composite, which simultaneously controls the modulus and practical dielectric permittivity of the dielectric layer to enhance the performance. Microengineering approaches can create micropatterns, micropores, and their combined structures in the dielectric layer.[198,203,204] By adjusting the parameters, such as size and distribution, the capacitive sensors achieve higher performance under pressure. For example, a porous structure for capacitive pressure sensors introduces $1-1000$ μm air bubbles in the dielectric layer to change the Young's modulus and permittivity. The silicon mold and PS beads could pattern the microstructure to achieve a higher sensitivity.[198] Figure 7a shows an experimental process to fabricate porous pyramid structures utilizing a combination of a pyramid and PS bead mold. At first, the PS beads gathered on the pyramid mold by utilizing blade coating. Then the mixed mold was transferred onto the PDMS precursor to fill the interspace of the mold. After curing, peeling, and dissolving the PS beads, the researcher could obtain the porous pyramid structure. Figure 7b,c shows the photo of the porous pyramid. The micropatterns also enhanced the detection limit, decreased the viscoelastic deformation, and accelerated the recovery. On the other hand, micropatterned electrodes can be an effective choice.[205−208] Like the dielectric design, the micropatterned electrodes obtain more enormous strains than the flat ones to increase the sensitivity of the sensor.

Some SEM images of micropatterns and micropores are shown in Figure 7d−g. Compared to the micropatterns, the micropores generate more significant changes in Young's modulus and effective permittivity. The porous capacitive pressure sensor is compressive under the same pressure.[209,210] But the effective Young's modulus is in constant growth with increasing strain. Kim et al. gave a detailed study on the process of compressing voids.[113] The results showed that the thin walls of the micropores folded under pressure, which increased the difficulty for further compression. With the same

porosity, the walls of larger pores with a lower modulus were easier to collapse, but leading to a slow recovery time probably. Also, the effective permittivity usually experienced a nonuniform increase with the compressed air voids.

3.2.3. Strain Sensing and Structural Designs. The strain sensor is an essential part of flexible and stretchable E-skins, including resistive and capacitive ones depending on the sensing mechanism. The strain sensors are used for monitoring tension, compression, and vibration, which describes the changes in mechanical conditions. For example, a typical resistive strain sensor transforms the mechanical deformation into the measured resistance change. The GF is defined as follows:

$$GF = \frac{\Delta R}{R_0 \varepsilon} \tag{3}$$

The R_0 is initial electrical resistance, ΔR is the relative change in R, and ε is the mechanical strain. Considering the applications for E-skins, strain sensors detect subtle physiological signals from elongation, compression, vibrations, and pressure variations. Also, strain sensors are appropriate to detect large deformation from biomechanical motions. The response and recovery time need to fit to monitor the mechanical changes.

The conductive pathways of resistive strain sensors are tuned by the tensile strains, which leads to the increasing resistance through the active part. Resistive strain sensors respond to the strains through connection breaking, crack propagation, and tunneling effect among the nanomaterials. The weak interactions among the nanomaterials and substrates will cause a mismatch in the mechanical properties.[211,212] The local stress induces the disconnections among the previously conductive points and the increase in the electrical resistance of the whole sensor. By monitoring the real-time resistive changes, the sensor can detect the corresponding strains quantitatively.[213] Multilayer strain sensors can also achieve the reversible slippery effect between connection and separation.[214,215] The microcracks appear in nanoparticles, nanowires, and thin flakes resulting from the concentrated stress along with stretched substrates.[216−219] The sensor generated cracks perpendicular to and shrinkages parallel to the stretching due to Poisson's ratio. These deformations will influence the cross-sectional area of the conductive pathways. Wang et al. synthesized graphene flakes/PVA fibers using the CVD method, which worked as a strain sensor with high sensitivity and stability.[220] The resistive changes were tuned by microcracks of graphene under strain. And there are possible tunneling conductive pathways that contribute to the whole electrical resistance in the strain sensor.[212]

Capacitive strain sensors occupy an essential position in E-skins.[110,221,222] The capacitive strain sensors sustain changes in the overlapping area and the thickness of the dielectric layer, which can be explained by the following equation:[189]

$$C_0 = \varepsilon_0 \varepsilon_r \frac{l_0 w_0}{d_0} \tag{4}$$

The C_0 is the initial capacitance, ε_0 is the vacuum permittivity, ε_r is the relative permittivity, l_0 is the initial length, w_0 is the initial width, and d_0 is the distance between the two electrodes equally the thickness of the dielectric layer.
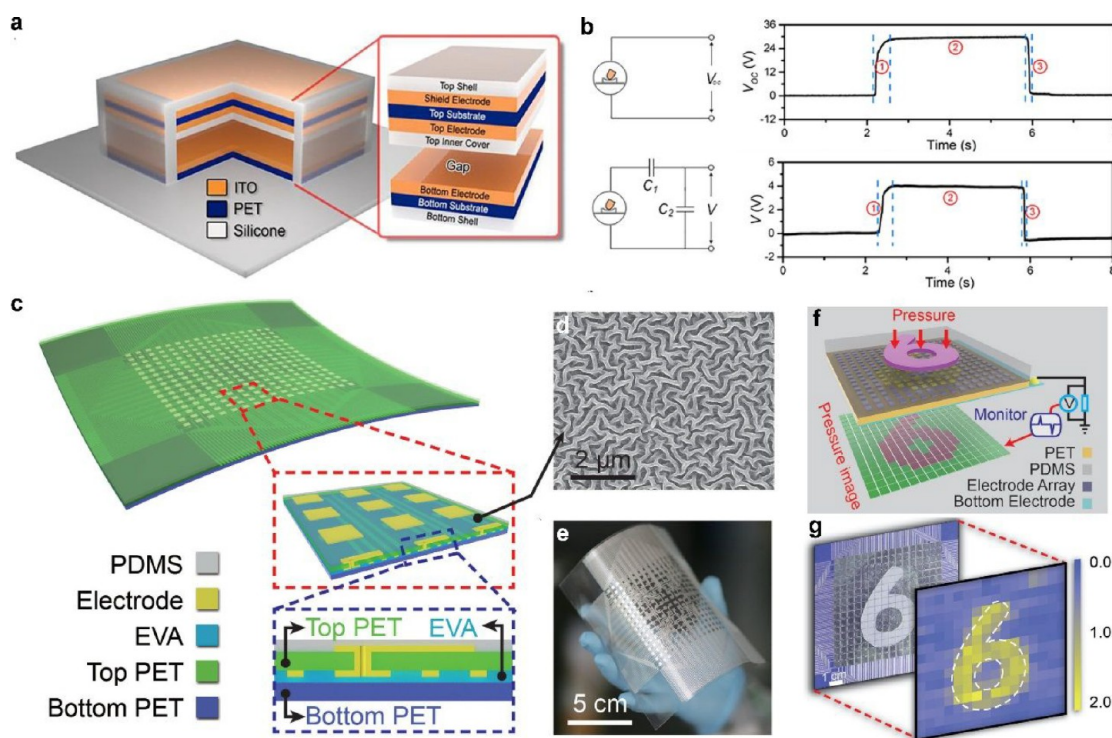
Figure 8. Self-powered sensors. (a, b) A self-powered keystroke system for rapidly recognizing the users' characteristics. Reproduced with permission from ref 235. Copyright 2018, Elsevier. (c) Schematic structure of the triboelectric sensor array. (d) SEM image of the etched PDMS surface. (e) Photograph of the sensors array. (f, g) Schematic illustration of pressure mapping and the results of the sensor array. Reproduced with permission from ref 236. Copyright 2016, Wiley.

$$C = \varepsilon_0 \varepsilon_r \frac{(1 + \varepsilon) l_0 (1 - v_{\text{electrode}}) w_0}{(1 - v_{\text{dielectric}}) d_0} = \varepsilon_0 \varepsilon_r \frac{(1 + \varepsilon) l_0 w_0}{d_0}$$

$$= (1 + \varepsilon) C_0 \tag{5}$$

And the stretchable strain sensor with the Poisson's ratio can be further given by the equation. The elongation will induce the corresponding changes in the width and distance at the same time. In this equation, the Poisson's ratio is perhaps not a constant value under a large-scale range of strains. Although capacitive strain sensors possess high stretchability, they exhibit low GF and sensitivity with a relatively slow change in the dielectric layer under horizontal tension.

3.2.4. Self-Powered Sensing and Structural Designs. The resistive and capacitive E-skins have achieved sensitive and sustainable detection for applied strain by employing micro-engineering and integration techniques. However, stably powering resistive and capacitive sensors is a challenge in fabricating flexible and stretchable E-skins. So the self-powered E-skins have attracted researchers' attention. They integrate energy storage or transducing functions, which can work without another external supply. Recently, self-powered sensors have been investigated based on photovoltaic, thermoelectric, and mechanical energy harvesting methods.[223−228] Compared to the photovoltaic and thermoelectric methods that the sensing components have to be activated by light and heat, the mechanical method provides the way for harvesting and transferring the mechanical energy from the nearby conditions to obtain electrical sensing signals. Tribo-electric nanogenerators (TENGs) have been one of the most promising self-powered devices to achieve E-skins.[229]

TENGs have been developed since 2012 and possess four working modes according to structural designs: vertical contact-separation, lateral sliding, single-electrode, and free-standing modes.[230,231] Each has its unique characteristics and should be appropriately chosen for specific applications or conditions. The basic principles of TENGs are based on the contact electrification for generating surface charges and Maxwell's displacement current for transferring mechanical energy into electrical signals. The surface charges will induce a potential difference between the two contact materials and their back electrodes. Then, mechanical motions can drive output current due to the surface polarization.[232] According to the mechanism of TENGs, they are appropriate for self-powered mechanical and biomechanical sensors. For example, the contact-separation mode TENG consists of two kinds of materials with back electrodes. When pressure is applied, the two materials contact each other to generate opposite surface charges due to the contact electrification. After releasing, the charged materials separate with a potential generated between the back electrodes, which further induces a current to balance the electrostatic charges. When the pressure is applied to the TENG again, there will be a current flowing in the opposite direction. In the whole process, a press will generate two alternative current pulses. And the signals can measure the intensity of the mechanical press.[233]

Some applications have been proposed for the TENGs to achieve HMI and E-Skins. Pu et al. fabricated a stretchable hydrogel-based TENG with the max elongation of 1160% and 96.2% transmittance.[234] The PAAm-LiCl hydrogel was encapsulated by PDMS and worked as a single-electrode TENG to detect pressure. Because of the softness and stretchability, the hydrogel-based TENG could be attached to complex surfaces and realized as an E-skin device. Wu et al. have developed a keystroke dynamics-based two-factor security

system.[235] The sensing part was composed of silicone rubber and PET-ITO based on the contact-separation mode. The desired voltage signals could be measured by typing for press and release, as shown in Figure 8a,b. During typing, the specific users' keystroke characteristics could be acquired by the signal intensity, holding time, and typing latency. With the help of the shielding electrode in the structure, the keyboard could achieve 98% accuracy for user authentication and identification based on machine learning. Wang et al. proposed a flexible triboelectric sensing array based on large-scale single-electrode TENGs.[236] The silver electrodes were on a piece of PET substrates. Another PDMS layer covered the surface as a triboelectric layer, as shown in Figure 8c−g. Each pixel size was down to $500 \times 500 \ \mu m.^2$ The fabricated device could achieve the functions of single touch, multipoint touch, and sliding press.

The TENG-based devices are different from those with other portable power supplies. Photovoltaic, thermoelectric, and energy storage devices harvest vital energy from the environment to drive sensors. These portable power supplies more usually power chemical sensors for health monitoring and tactile sensors for E-skins. However, the TENGs can directly respond to external mechanical stimulations, such as pressure and strain. The TENG's pulse currents can be utilized as direct sensing signals without extra components. Some researchers even explore the method of utilizing TENG to power other small electronics. From this point, TENG-based sensors are different from resistive and capacitive sensors. However, they share similar structural designs to improve the performance, such as microengineering and stretchable conductors.

3.3. Key Parameters and Improvement Strategy: Sensitivity, Threshold, Linearity, Resolution. *Sensitivity.* Sensitivity is defined as the slope of the electrical sensing response upon the applied pressure or strains, which manifests the measuring capacity of the sensor. The realization of higher sensitivity can effectively enhance the response to stimuli to obtain higher accuracy. Various attempts have been increasing the sensitivity of the E-skin devices, most of which are improvements of materials, structural designs for mechanical properties, and novel mechanisms at the micro-/nanoscale. For example, the shapes of active materials can tune the sensing performance of resistive sensors. The tension will influence the sharp and continuous changes in resistance for the 1D nanowires. Also, the structural designs of the active layer contribute to the sensitivity to external pressure. The micropatterns on the surface and the micropores inside the layers will enlarge the strains under the same pressure.

Detecting limit and effective range. The detection limit describes the lowest value for distinguishing the step change of electrical signals under external stimuli. It is usually the minimum stimuli that a sensor can respond to, which is essential for practical applications and subtle requirements. The effective detecting range reflects the mechanical limits of sensors. Excessive pressure exceeding the limit can lead to stress failure in the structure. And the compression simultaneously strengthens the Young's modulus of the device to decrease the sensitivity to strain. It is in the effective detecting range that sensors can effectively give out electrical responses to external stimuli without exceeding the physical limits. For the majority of flexible sensors, both mechanical properties and sensing mechanisms determine the actual use

range. Many efforts have been devoted to the exploration of appropriate sensors to satisfy the specified range.

Linearity. Linearity is an essential parameter to achieve better detecting performance and integration for the tactile sensors. The high linearity of electrical responses to stimuli will effectively reduce the complexity of information, further decreasing the cost of signal processing circuits and calibration. Simultaneously, the linearity of responses is contributed to machine learning to develop smart sensors with the help of artificial intelligence. The linear response is mainly due to the rational design, which usually appears in simple-structured pressure or strain sensors.[110]

Resolution. The distribution of sensing units on a device will determine the spatial resolution when recognizing the pressure or strain mapping. For a tactile sensor, distinguishing the distance of the sliding trajectory and the multipoint contact pressure are both essential capacities. By developing designs and techniques for high resolution, E-skins can achieve naturally skin-like properties and broaden future applications.

4. DESIGN AND INTEGRATION STRATEGIES: FLEXIBLE AND SCALABLE INTEGRATED SENSING SYSTEM

The design and integration of sensors for E-skins are exceedingly significant for establishing real-time sensing systems. This section mainly reviews the latest progress in fabricating E-skins of various types, including sensor arrays, multifunctional sensor platforms, HMIs, self-powered devices, integrating data processing, storage, and transmission modules.

4.1. Sensor Array: Pressure Mapping or Track Recognition. A sensor array has been developed based on the matrix of sensing units, including pressure and strain sensors, to achieve pressure mapping or track recognition. A sensing unit as a sensing pixel occupies a small area of the device. So the accurate detection of human motion and tactile sensing is based on the high spatial resolution of sensing units. The spatial resolution requires appropriate designs to decrease the heavy burdens of data acquisition and the complexity of conductive circuits for various applications. For instance, the sensor array to mimic a fingertip touch may need to satisfy a spatial resolution of 1 mm. However, for the joints and palms, the requirement is much lower.

According to the reading methods, the sensing units fabricating the sensor array are typically two classes of active[237−240] and passive[110,241−243] sensors. In the active sensor array, each sensing unit matches an individual switch to address itself. This approach remains discrete circuits for sensing units, effectively reduces the noise and power consumption, and most significantly improves the response time. However, the large transmitting and processing components for sensors increase the complexity and convenience of the sensor array. While the passive sensor array decreases the structure of addressing by identifying the row and column position of the sensing unit, the passive method simplifies the device structure. However, it faces challenges in crosstalk, response time, and multipoint operation. Besides electrical monitoring, the combination of visualization is also a solution to cut down the number of conductive lines.[238] Wang et al. proposed a dual-function sensor array with high sensitivity and resolution for electrical and optical pressure mapping simultaneously.[36] The fabricated full dynamic-range pressure sensor matrix (PSM) consisted of two separate parts of the single-electrode TENG matrix and
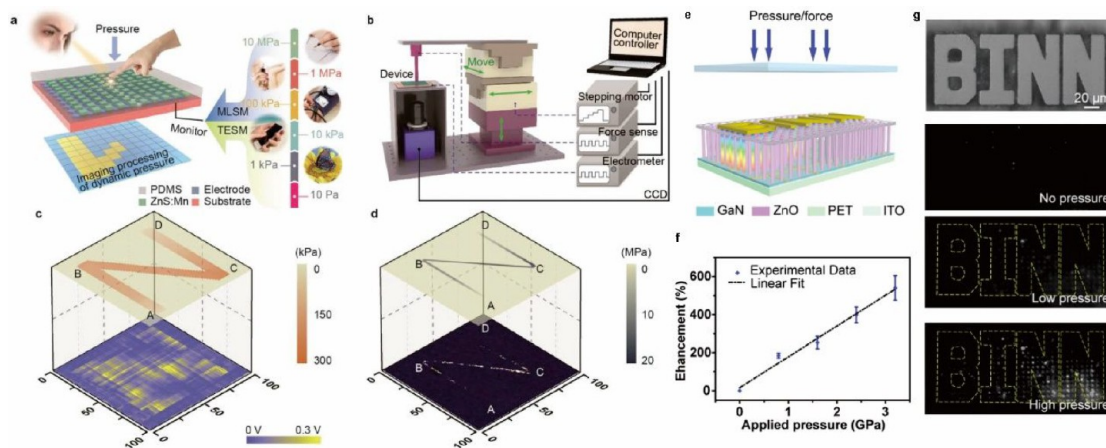
Figure 9. Sensor array. (a, b) Schematic illustration of optical and electrical dual-mode sensing. (c, d) The sensing results of the electrical signals and optical signals. Reproduced with permission from ref 36. Copyright 2017, Wiley. (e) Schematic of the strain-induced pressure sensor array. (f) The strain-induced enhancement in intensity. (g) Photos were captured under different strains. Reproduced with permission from ref 244. Copyright 2019, Elsevier.
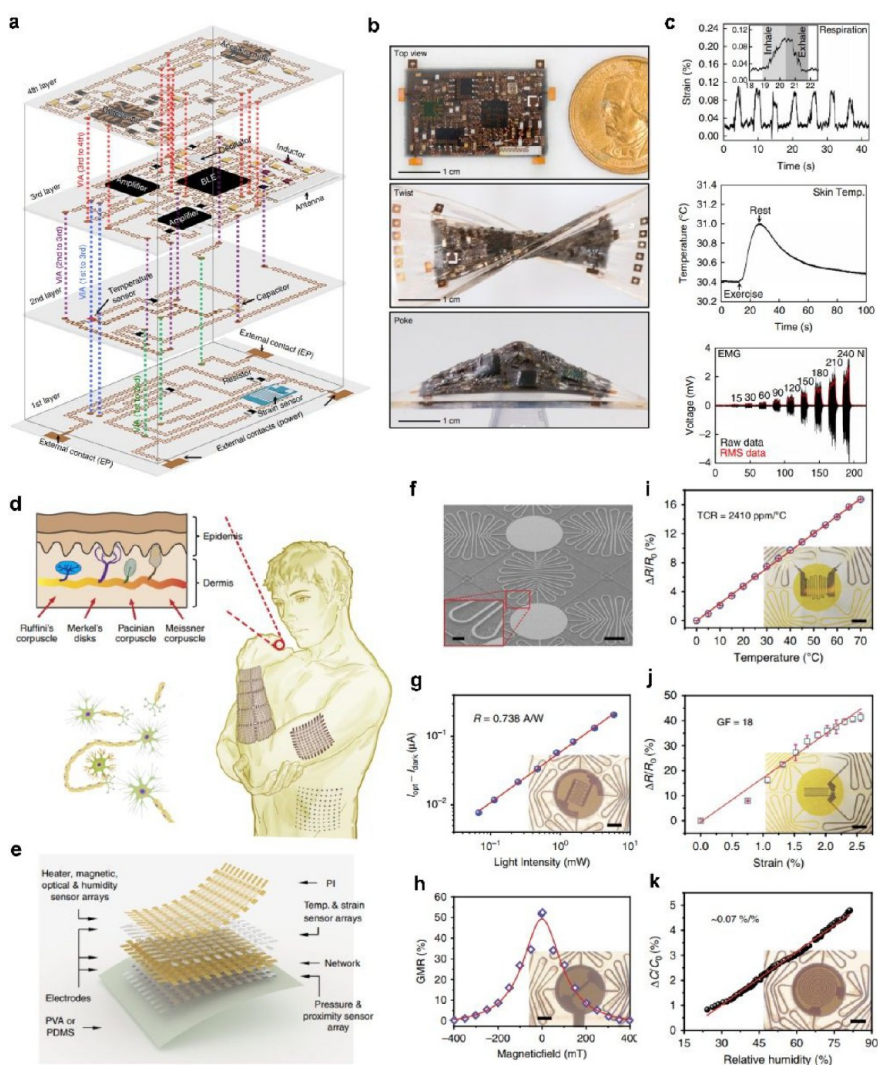

Figure 10. Multifunctional sensor platform. (a) Schematic of the 3D framework of the stretchable system. (b) The corresponding photos. (c) Sensing signals of the bending strain, skin temperature change, and EMGs. Reproduced with permission from ref 39. Copyright 2018, Springer Nature. (d, e) The schematic of the SCMN. (f) The SEM photo of the SCMN. (g–k) Multifunctional sensing performances of ultraviolet light, magnetic field, temperature, in-plane strain, and relative humidity. Reproduced with permission from ref 256. Copyright 2018, Springer Nature.
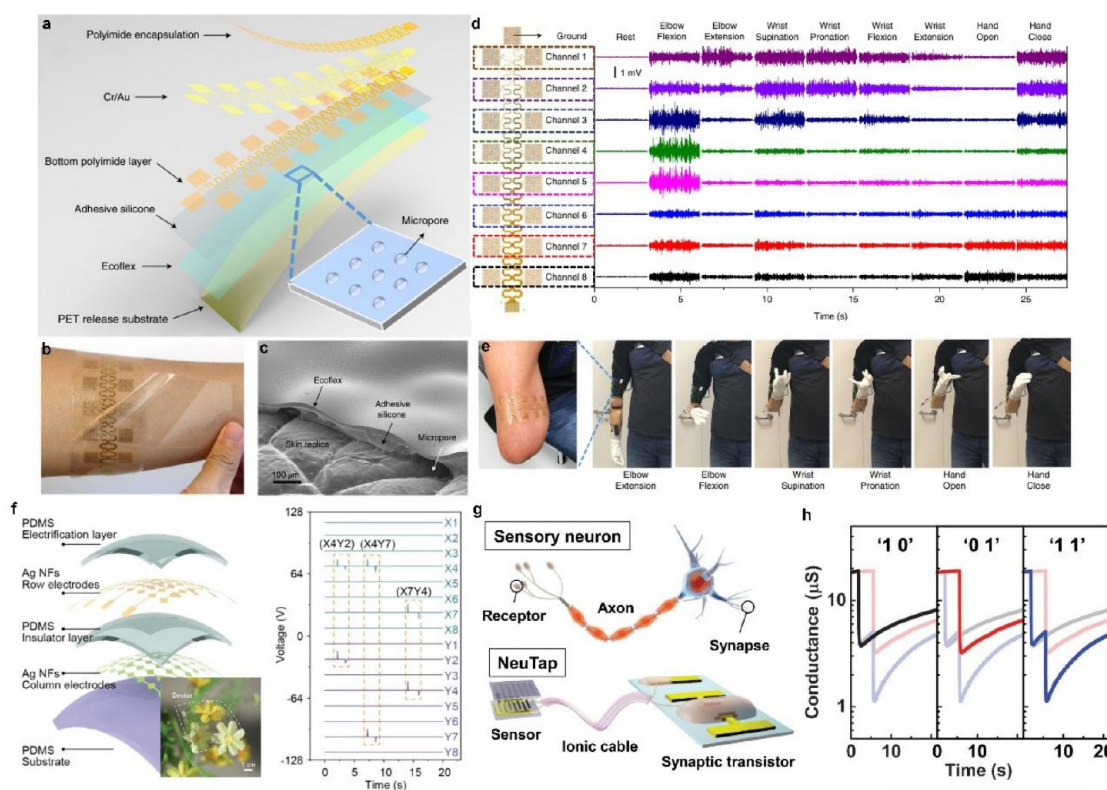
Figure 11. HMIs. (a) The structure of the epidermal electrical interface. (b, c) Photo of the device on the arm and SEM image of the adhesive layer. (d, e) Photos of the large-area epidermal electrodes and multichannel EMG for prosthetic control. Reproduced with permission from ref 37. Copyright 2019, Springer Nature. (f) Schematic structure of the TETS array to recognize the sliding motion. The inset is the photo of the device. Reproduced with permission from ref 242. Copyright 2018, Wiley. (g) The schematic illustration of NeuTap. (h) Typical responses of the NeuTap to three types of pattern pairs. Reproduced with permission from ref 258. Copyright 2018, Wiley.

mechanoluminescent sensor matrix in vertical integration. And the matrix covered sensing regimes of 0.6−200 kPa with electrical sensing and 0.65−30 MPa with visible sensing, shown in Figure 9a. The TENG matrix consisted of the micropatterned PDMS and the rows and columns of the electrode array. And the mechanoluminescent matrix was an array of ZnS: Mn/photoresist composite squares. The cross-bar electrodes were on the substrate in the experiment, with the mechanoluminescent matrix on the top. Then PMMA was spin-coated as a protection layer, followed by the micro-patterned PDMS onto the whole device. The single TENG sensor and single mechanoluminescent sensor realized a sensitivity of 6 MPa^{-1} and 0.037 MPa^{-1} and the response time of 50 and 9.23 ms, respectively. The authors fabricated the PSM with 100 × 100 sensing pixels and 100 dpi resolution to demonstrate the real-time pressure and track recognition through simultaneously electrical and visible signals. Figure 9b shows the schematic illustration of the working PSM and its measurement setup of a stepping 3D motor and a force detector. The system controlled the object to slide on the surface of the device. And the sliding track was the same as the shape of "N" from the A to D positions. The corresponding results of electrical and optical signals are in Figure 9c,d. During the process, the self-developed software could display the spatial pressure distribution through the voltage and light intensity of each pixel sensor.

Peng et al. developed another strain-induced pressure sensor array.[244] The device was based on the heterostructure of the p-GaN/n-ZnO LED to realize the large-scale and spatial pressure mapping. The flexible GaN film was grown on the sapphire substrate and then lifted off by a high-power laser beam. Then the GaN film was transferred on the PET substrate, with the p-doped surface facing outward. The ZnO nanowires epitaxially grew with the help of photolithography and hydrothermal methods. The fabricated p-GaN/n-ZnO LED array followed the mechanism of piezo-phototronics.[245−250] The applied pressure on the LED could induce piezoelectric polarization charges on the p−n junction to enhance the corresponding electroluminescence intensity. The sensor array achieved the pressure mapping with a high resolution of 2.6 μm and a response time of 180 ms by associating the pressure and light intensity. As Figure 9e displays, a microscale and convex stamp pressed on the LED array to induce piezoelectric potential along the length of the ZnO nanowires. The applied pressure tuned the enhancement of emission intensities and displayed a linear relationship with the enhancement factor E, which reached 530% under over 3 GPa for the nanowires in Figure 9f. The photos in Figure 9g illustrate the prolonged visualization of pressure based on the progressive changes in intensities. In this way, the sensor array could reveal the distribution of pressure on the device.

4.2. Multifunctional Sensor Platform: Integrating Functions. Minimizing the size of sensing units to maximize the integration density on a single device requires an experienced design. Multifunctional sensors or multimodal sensing for different parameters, such as strain, pressure, temperature, and humidity are based on various mechanisms and physical configurations to monitor the external signals. Although it is possible to integrate the functional components on a single layer or integrate all functions into one unit, the

device is more likely to face a bottleneck on the design and other fabricating constraints.[251,252] So functional components have been integrated into the stacked structure to enhance the density and mimic the sensing capability of human skin.[253−255]

Huang et al. fabricated a 3D framework for integrating a stretchable system with interlayer electrical connections.[39] The stretchable device was established in a four-layer structure with an island-bridge design for each layer to release the mechanical stress under strain, shown in Figure 10a. And the electrical connections among the layers were through the vias formed by controlled laser ablation and soldering with conductive materials. As for every single layer, the bilayers of Cu/PI thin films connected the distributed functional components of resistors, capacitors, inductors, amplifiers, and radiofrequency components. Then an ultralow modulus silicone encapsulates the layers for mechanical robustness and stretchability. The fabricated device achieved an elongation of 50%, 35%, and 20% in the vertical, horizontal, and equal-biaxial directions, respectively. The device could work to sense the bending strain, skin temperature, and EMGs, as shown in Figure 10c.

Hua et al. developed a sensor matrix with multifunctional sensing functions.[256] The fabricated highly stretchable and conformable matrix network (SCMN) provided simultaneous recognitions for several types of environmental information, shown in Figure 10e. The device possessed a multilayer structure, of which each layer was an island-bridge design. The whole device consisted of 100 sensory nodes connected by serpentine wires, with functional sensing units discretely distributed in the layers. Figure 10f shows the SEM image of the sensory nodes. The connections were critical to realize the expansion of the SCMN. The results showed that the wire could sustain a strain of 800% with a lower than 2.6% decrease in the resistance. So the fabricated device possessed large-area expandability and was suitable for complex 3D integration and positioning the nodes at specific sites. More than the sensing of pressure and proximity, the SCMN had the functions of sensing ultraviolet light, magnetic field, temperature, in-plane strain, and relative humidity, as shown in Figure 10g−k. And the authors displayed the pressure and temperature mapping on an intelligent prosthetic hand when grasping.

4.3. HMIs: Transferring Signals and Machine Learning. HMIs promote two-way communication between humans and computers or machines through induction and feedback.[257] With the help of HMIs, the information on the human skin or other bodies can be obtained and further transferred into feedback as electrical, visual, audio stimulations, and so on. Several researchers have focused on improving adaption to complex surfaces and movements, including prosthetic limb control, machine learning, and virtual object control.

Tian et al. fabricated an epidermal electrical interface that could record electrophysiological signals.[37] The device was a two-layer design with a large area and multifunctions, as shown in Figure 11a. The functional mesh electrodes with Greek shapes were on the PI film, interconnected by filamentary serpentine wires. Another PI encapsulation was on the wires to guarantee insulation. Adhesive silicone provided robust adhesion for the whole device on the human skin. The silicone layer featured adjustable micropores by dissolving the PMMA microspheres to enhance the air permeability and bonding of the device. Then, an Ecoflex silicone film and a removable PET sheet were for transferring the epidermal interface. The Ecoflex and PET could be easily peeled off and leave the bonded interface on the skin, as shown in Figure 11b. The SEM image

of the adhesive layer is displayed in Figure 11c. The authors utilized the epidermal interfaces to cover the forehead, scalp, and entire circumference of the arm. The area was primarily improved. Moreover, they achieved advanced applications in multimodal prosthetic control with simultaneous magnetic resonance imaging (MRI) and EMG/EEG. A male with a right transhumeral amputation and targeted muscle-reinnervation surgery utilized the epidermal EMG array to control the robotic prosthesis. The experiment showed a behavior recognition accuracy of 89% after data collection and machine training.

A self-powered triboelectric tactile sensor (TETS) was achieved by Wang et al. using silver nanofibers (AgNFs) as electrodes and elastomers as substrates.[242] They first synthesized PVA nanofibers through electrospinning, and then covered the PVA fibers with a thin layer of silver to obtain the AgNFs. The fabricated AgNFs were transferred onto a layer of PDMS. They were treated with photolithography and etching to form conductive patterns, further encapsulated by another layer of PDMS. In the spinning process, the orientation and density of the nanofibers were carefully controlled, which had a significant impact on conductivity, transmittance, and stretchability. The TETS achieved a sheet resistance of 1.68−11.1 Ω^{-1} with over 70% transmittance. Moreover, the authors demonstrated the synthesis of unidirectional, bidirectional, tridirectional, and random nanofibers. The directions possessed different conductivities according to the angles of stretching. For example, the results showed that the resistance only increased by 10% for random AgNFs under 100% strain. PDMS encapsulation on the device could work as a triboelectric layer for the single-electrode TENG. The TENG response time was about 70 ms, which could constitute a sensor matrix in Figure 11f on a human arm to input signals to communicate with the computer software to play Pac-Man.

Wan et al. developed a neuromorphic tactile processing system (NeuTap) combined with a pressure sensor and ionic-gated synaptic transistor.[258] The NeuTap could work as mechanoreceptors, axons, and synapses to mimic sensory neurons of humans for perceptual learning. The resistive pressure sensor utilized the CNTs-coated micropatterned PDMS as the active layer. And the interdigital electrodes were on the PET film to provide the two terminals of the sensor. One of the terminals connected to gate the indium-tungsten-oxide (IWO) channel through PVA ionic cables. And the applied pressure could induce the changes in resistance in series with the ionic gate, which further influenced the gate voltage. The corresponding illustration is in Figure 11g. The authors demonstrated the NeuTap neuron to implement tactile recognition for convex and flat patterns. In Figure 11h, a finger touched the patterns to obtain the corresponding binary code with the NeuTap. The pressure induced by the convex "1" and flat "0" changed the synaptic weight, which could be for machine learning and intelligent recognition.

4.4. Self-Powered Devices: TENG and Wearable Power Source. Various kinds of sensors and modules need power supplies to constitute the systems. But extra power packages increase the burden on the weight and structure of the device. From this point, powering flexible and stretchable sensors is required to satisfy stability, steadiness, comfort, and convenience. The method of integrating a self-powered power supply, such as TENG and a wearable power source, has been
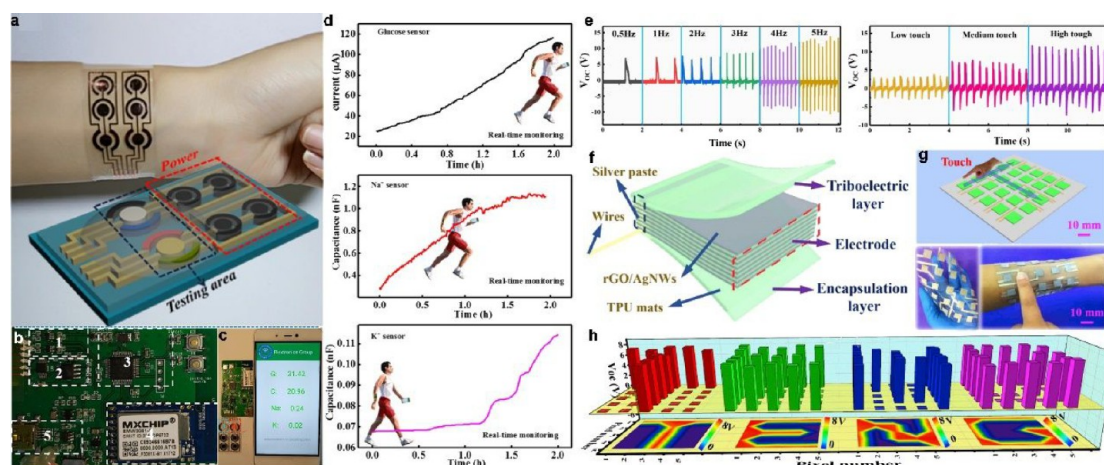
Figure 12. Self-powered devices. (a, b) Photo and schematic image of the self-powered sweat system for the glucose, [Na$^+$], and [K$^+$]. (c, d) Photo of wireless PCB and corresponding outputs. Reproduced with permission from ref 38. Copyright 2019, Elsevier. (e) The real-time monitoring curves of the device. (f) Self-powered e-skin in tactile sensing and energy harvesting. (g) The schematic image and photo of the sensor. (h) The tactile sensing results from the sensor array. Reproduced with permission from ref 259. Copyright 2020, Elsevier.

developed to overcome the challenges of realizing independent or portable power for real-time sensing.

Lu et al. reported a self-powered sensing system by integrating sensor arrays of a glucose sensor, [Na$^+$] and [K$^+$] selective sensors with micro-supercapacitors (MSCs) on a PET film.[38] The system was based on concentric circular structured electrode arrays, which were fabricated with photolithography on the PET film and provided for conductive pathways between the sensors and MSCs. An Al$_2$O$_3$ layer covered the electrodes and guaranteed insulation except for the area of the sensors and MSCs. Then the precursors of sensors and MSCs were onto specific positions for discrete functional areas. Schematic illustration and photo of the fabricated device on the arm are displayed in Figure 12a. The MSCs possessed an areal capacitance of 18.5 mF cm^{-2} to continuously power the sensors for real-time monitoring with the help of a voltage regulator. The sensors could monitor the varied concentration, among which the glucose sensor achieved a sensitivity of 0.5 A/M. A prototype system for personalized health monitoring demonstrated the application of the integrated device, as shown in Figure 12b,c. The device could analyze the in situ concentration of glucose [Na$^+$] and [K$^+$], which was possible to achieve a self-powered sweat monitoring system by analyzing metabolic perspiration.

Zhou et al. fabricated highly stretchable flexible and multilayered nanofiber mats as E-skin.[259] In the structure, TPU nanofibers were fabricated by electrospinning to obtain stretchable, breathable, and light nanofiber mats. During the spinning process, the rGO and AgNW solutions were sprayed on the TPU mats as conductors. The device worked based on the single-electrode TENG and demonstrated its self-powered performance in Figure 12e. The whole structure displayed an alternant layered structure with repetitively fabricating TPU mats and conductive layers to establish stable conductive paths separately, as shown in Figure 12f. The device was based on the single-electrode TENG and worked as a self-powered sensor with up to 200 V output voltage and a sensitivity of 78.4 kPa^{-1} when applied pressure was lower than 2 kPa. The sensor array was attached to the arm in the experiment, as shown in Figure 12g. It realized the pressure mapping on the plane and enabled the potential applications of HMIs, as shown in Figure 12h.

4.5. Integrating Data Processing, Storage, and Transmission Modules: Wireless Transmission and Real-Time Sensing.
In-plane interconnections and vertical integration are two strategies to integrate functional electronic components and construct flexible and stretchable sensing systems. According to the deformation that the circuits bear, conventional conductive tapes, wires, and flexible conductive methods described in the previous sections are typical approaches to provide the conductive connections among the different components, according to the deformation that the circuits bear. When establishing the vertical multilayer structure, deformable vias are needed to connect among the layers.[260−262] Although fully flexible sensing systems face challenges due to the physical limitations of rigid electrical components, the rapid development in flexible electronics will attract significant attention and research efforts for potential applications.

Li et al. demonstrated an ultrathin crack-based sensor for detecting strain deformation, with signal acquisition circuits and real-time display.[263] The integrated sensor and process system provided a method for precise tactile control. The PDMS film was transferred to the PET substrate by dissolving the sacrificial layer. Then the silver nanolayer was deposited by magnetron sputtering on the PDMS. The PET was bent to introduce the cracked structure in the silver electrodes. The strain sensor realized a high GF of 44013 at a strain of 0.88% and a low detection limit for 0.01% elongation. The authors further fabricated a visually aided tactile enhancement system with devices on the gloves, as shown in Figure 13a−c. The visually aided tactile enhancement system comprises an ultrathin strain sensor array, a multichannel signal acquisition device, a wireless serial port, and a real-time display program. The system has potential applications for assistance in precise tactile control. The system also enabled real-time and ultrasensitive sensing for slight deformation from a slight water drop, a feature, and invisible wires. The corresponding results of sensing the slight feather from different fingers and invisible wires are shown in Figure 13d,e.

Tao et al. fabricated a vertical through-hole dielectric layer for building a capacitive pressure sensor array.[264] The experiment optimized the sizes and structural configurations of the holes. The results showed that the fabricated sensor
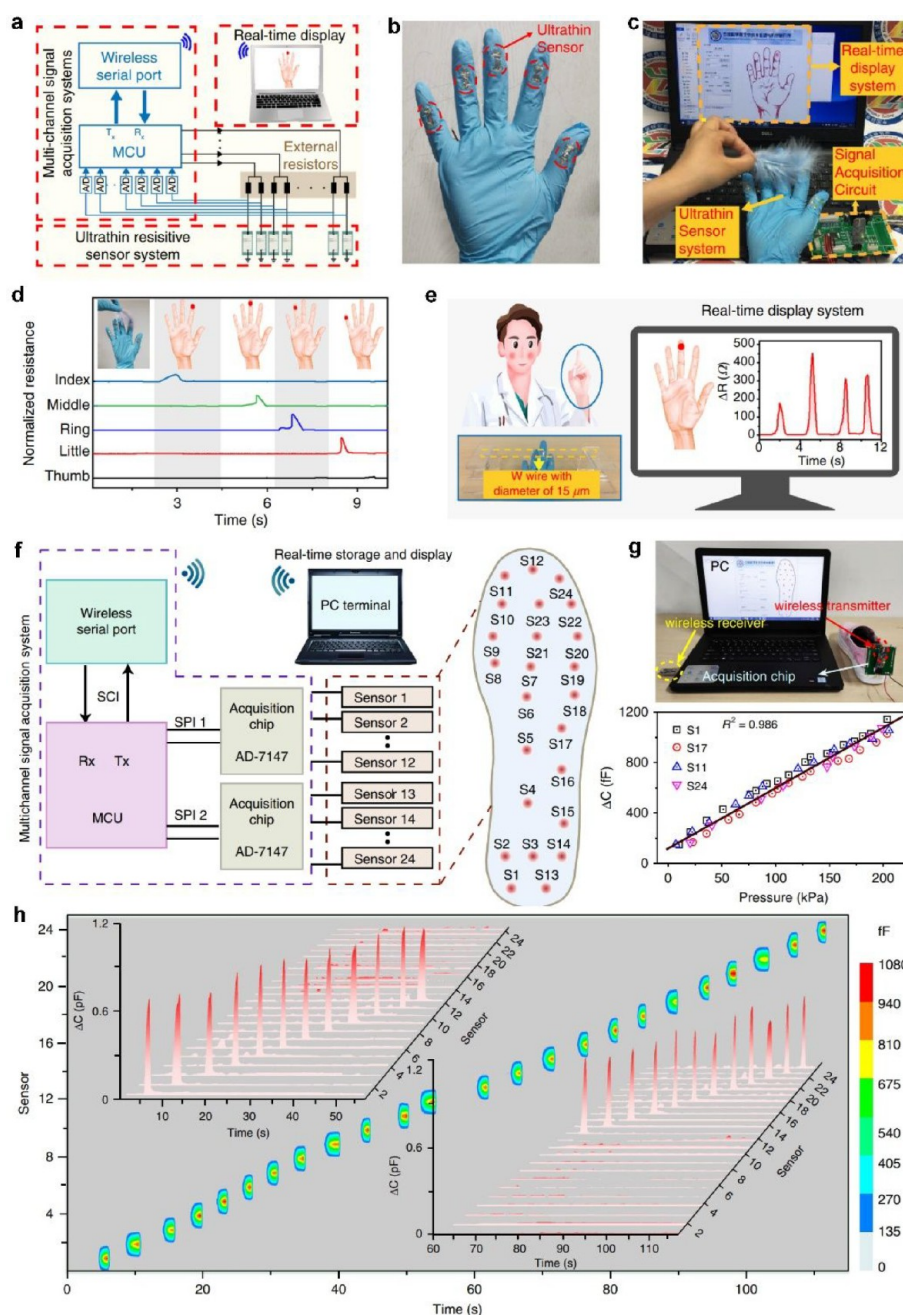
Figure 13. Integrating data processing, storage, and transmission modules. (a) Schematic illustration of the multichannel signal acquisition circuit and wireless system. (b, c) Photograph of the glove with sensors and detecting the soft feather. (d) The response sensors on each finger and corresponding results. (e) Detecting the touch of invisible wire, and visually getting tactile information. Reproduced with permission from ref 263. Copyright 2020, AIP Publishing. (f) Principal schematic of the smart insole system with 24 channels, DAQ circuit, and wireless modules. (g) Photograph of the system and the real-time monitoring curve. (h) The display of the results from 24 channels. Reproduced with permission from ref 264. Copyright 2020, Springer Nature.

achieved excellent linearity and stability in the range of 0−200 kPa. And the sensor achieved the highest sensitivity of 12 × 10^{-3} kPa^{-1} with hexagonal-distributed holes of 600 μm. Furthermore, the capacitive pressure sensor array constructed a smart insole system to monitor plantar pressure mapping, as shown in Figure 13f. The system consisted of 24 capacitive sensors distributed on the insole, a data acquisition, a wireless transmitter, a wireless receiver, and a PC with a real-time processing program. In the experiments, the authors displayed the system that recognized the static and dynamic pressure distributions in standing, yoga asana, walking straight, turning

around, falling, and going upstairs. The system could distinguish the pressure from each sensor to build the pressure mapping. The data could be obtained through each of the channels to achieve real-time monitoring in Figure 13h.

5. CONCLUSIONS

Flexible and stretchable E-skins and their representative applications are highlighted in this review. The rapid and sensitive monitoring of external activities has provided new sensors in wearable devices, health monitors, prosthetics, robotics, and HMIs. Through interdisciplinary collaborations,

flexible and stretchable E-skins can translate from research to products and benefit people. Recent advances in flexible and stretchable E-skins are on various materials. Nanomaterial-enabled sensors have been demonstrated with high sensitivity and mechanical stability. Material synthesis techniques, which are controllable and stable, are significant for developing new E-skins with self-healing, biodegradability, and gas-permeability to enhance comfort and convenience. Also, low-cost and rapid methods are essential for scalable manufacturing. Selective detection of functional nanomaterials is appropriate for the chemical, humidity, temperature, UV light, and other conditions. However, long-term cytotoxicity should be avoided for biocompatibility. Substrates are still in need of further development to support functional materials. Flexible and stretchable polymers are common and plastic substrates with stable mechanical properties for achieving deformable conformability. The combination of nanomaterials and substrates can determine the basic structural designs of the device. Moreover, transparency, heat tolerance, and chemical tolerance are also significant properties in satisfying fabrication process requirements and applications.

Besides the progress in nanomaterials, the achievements of the mechanism and structural designs play significant roles in realizing the sensing functions. Microengineering is the primary approach to introduce the microstructures in the active and dielectric layers. Many efforts are devoted to developing the structures of micropatterns, micropores, multilayers. The microstructure could tune the mechanical and electrical properties, which improves the performance of the tactile sensors. The layers can be uniform or composites with nanomaterials. Each layer provides specific properties in establishing resistive, capacitive, and self-powered sensors. They impact the sensitivity, effective working range, detection limit, response time, relaxation time, and so on. Designs remain to be further explored for improving the properties of the active or dielectric layers, especially considering large-scale and commercial uses.

Compared to resistive and capacitive sensors, self-powered devices have advantages in energy consumption. Mechanical, sunlight, thermal, and chemical energy from the external environments can provide portable power supporting the sensors based on integrated energy harvesters. However, wearable energy harvesters are limited by the specialized conditions and activities, including the positions of the harvester and the level of mechanical activities of the body or environment, which are impracticable to provide continuous and stable power. So the developments on self-powered sensors are emerging to satisfy the requirements of power supply. In the other aspect, the flexible and mobile storage devices of batteries and supercapacitors are potential alternatives for the flexible sensors.

Despite remarkable progress in sensors, flexible and stretchable electrical components are still at their initial stages, such as signal processing, data storage, and transmitting devices. For the majority of applications, sensing information relies on the processing of external modules. Because of the incompatibility of inorganic electronics with stretchable sensors, the integration density of the whole devices is still low. The integration density can be improved by in-plane integration of heterogeneous components, including wavy, island-bridge, and other methods to achieve the stretchable systems, and by a 3D stacked structure through VIAs. However, innovative designs in scalable and low-cost fabrication and the thermal and electrical invalidation that arise from long-term operation have attracted attention. Incorporating wireless communication modules allows for remote transmission. With flexible electronics and enhanced power technologies, the E-skins will support the IoT soon.

■ AUTHOR INFORMATION

Corresponding Authors

Caofeng Pan − *CAS Center for Excellence in Nanoscience, Beijing Key Laboratory of Micro-Nano Energy and Sensor, Beijing Institute of Nanoenergy and Nanosystems, Chinese Academy of Sciences, Beijing 100083, P. R. China;* orcid.org/0000-0001-6327-9692; Email: cfpan@binn.cas.cn

Wenchao Gao − *Department of Civil Engineering, Monash University, Clayton 3800, Australia;* Email: wenchao.gao1@monash.edu

Authors

Zuqing Yuan − *CAS Center for Excellence in Nanoscience, Beijing Key Laboratory of Micro-Nano Energy and Sensor, Beijing Institute of Nanoenergy and Nanosystems, Chinese Academy of Sciences, Beijing 100083, P. R. China; Institute of Microscale Optoelectronics, Shenzhen University, Shenzhen 518060, PR China;* orcid.org/0000-0003-3988-0618

Su-Ting Han − *Institute of Microscale Optoelectronics, Shenzhen University, Shenzhen 518060, PR China;* orcid.org/0000-0003-3392-7569

Complete contact information is available at:
https://pubs.acs.org/10.1021/acsaelm.1c00025

Notes

The authors declare no competing financial interest.

■ REFERENCES

(1) Wang, B.; Huang, W.; Chi, L.; Al-Hashimi, M.; Marks, T. J.; Facchetti, A. High-k gate dielectrics for emerging flexible and stretchable electronics. *Chem. Rev.* **2018**, *118* (11), 5690−5754.

(2) Bao, Z.; Chen, X. Flexible and stretchable devices. *Adv. Mater.* **2016**, *28* (22), 4177−4179.

(3) Liu, Y.; Pharr, M.; Salvatore, G. A. Lab-on-skin: a review of flexible and stretchable electronics for wearable health monitoring. *ACS Nano* **2017**, *11* (10), 9614−9635.

(4) Zhan, Y.; Mei, Y.; Zheng, L. Materials capability and device performance in flexible electronics for the Internet of Things. *J. Mater. Chem. C* **2014**, *2* (7), 1220−1232.

(5) Hammock, M. L.; Chortos, A.; Tee, B. C. K.; Tok, J. B. H.; Bao, Z. 25th anniversary article: the evolution of electronic skin (e-skin): a brief history, design considerations, and recent progress. *Adv. Mater.* **2013**, *25* (42), 5997−6038.

(6) Kanao, K.; Harada, S.; Yamamoto, Y.; Honda, W.; Arie, T.; Akita, S.; Takei, K. Highly selective flexible tactile strain and temperature sensors against substrate bending for an artificial skin. *RSC Adv.* **2015**, *5* (38), 30170−30174.

(7) Trung, T. Q.; Lee, N. E. Flexible and stretchable physical sensor integrated platforms for wearable human-activity monitoring and personal healthcare. *Adv. Mater.* **2016**, *28* (22), 4338−4372.

(8) Yu, C.; Masarapu, C.; Rong, J.; Wei, B.; Jiang, H. Stretchable supercapacitors based on buckled single-walled carbon-nanotube macrofilms. *Adv. Mater.* **2009**, *21* (47), 4793−4797.

(9) Castro, H.; Correia, V.; Sowade, E.; Mitra, K.; Rocha, J.; Baumann, R.; Lanceros-Méndez, S. All-inkjet-printed low-pass filters with adjustable cutoff frequency consisting of resistors, inductors and transistors for sensor applications. *Org. Electron.* **2016**, *38*, 205−212.

(10) Wu, B.; Heidelberg, A.; Boland, J. J. Mechanical properties of ultrahigh-strength gold nanowires. *Nat. Mater.* **2005**, *4* (7), 525−529.

(11) Zhu, T.; Li, J. Ultra-strength materials. *Prog. Mater. Sci.* **2010**, *55* (7), 710−757.

(12) Richter, G.; Hillerich, K.; Gianola, D. S.; Monig, R.; Kraft, O.; Volkert, C. A. Ultrahigh strength single crystalline nanowhiskers grown by physical vapor deposition. *Nano Lett.* **2009**, *9* (8), 3048−3052.

(13) Kim, D.-H.; Lu, N.; Ma, R.; Kim, Y.-S.; Kim, R.-H.; Wang, S.; Wu, J.; Won, S. M.; Tao, H.; Islam, A. Epidermal electronics. *Science* **2011**, *333* (6044), 838−843.

(14) Webb, R. C.; Bonifas, A. P.; Behnaz, A.; Zhang, Y.; Yu, K. J.; Cheng, H.; Shi, M.; Bian, Z.; Liu, Z.; Kim, Y.-S.; Yeo, W.-H.; Park, J. S.; Song, J.; Li, Y.; Huang, Y.; Gorbach, A. M.; Rogers, J. A. Ultrathin conformal devices for precise and continuous thermal characterization of human skin. *Nat. Mater.* **2013**, *12* (10), 938−944.

(15) Xu, J.; Wang, S.; Wang, G.-J. N.; Zhu, C.; Luo, S.; Jin, L.; Gu, X.; Chen, S.; Feig, V. R.; To, J. W. Highly stretchable polymer semiconductor films through the nanoconfinement effect. *Science* **2017**, *355* (6320), 59−64.

(16) Oh, J.; Yang, J. C.; Kim, J.-O.; Park, H.; Kwon, S. Y.; Lee, S.; Sim, J. Y.; Oh, H. W.; Kim, J.; Park, S. Pressure insensitive strain sensor with facile solution-based process for tactile sensing applications. *ACS Nano* **2018**, *12* (8), 7546−7553.

(17) Gao, W.; Emaminejad, S.; Nyein, H. Y. Y.; Challa, S.; Chen, K.; Peck, A.; Fahad, H. M.; Ota, H.; Shiraki, H.; Kiriya, D.; Lien, D.-H.; Brooks, G. A.; Davis, R. W.; Javey, A. Fully integrated wearable sensor arrays for multiplexed in situ perspiration analysis. *Nature* **2016**, *529* (7587), 509−514.

(18) Shin, S.-H.; Ji, S.; Choi, S.; Pyo, K.-H.; Wan An, B.; Park, J.; Kim, J.; Kim, J.-Y.; Lee, K.-S.; Kwon, S.-Y.; Heo, J.; Park, B.-G.; Park, J.-U. Integrated arrays of air-dielectric graphene transistors as transparent active-matrix pressure sensors for wide pressure ranges. *Nat. Commun.* **2017**, *8* (1), 1−8.

(19) Lim, S.; Son, D.; Kim, J.; Lee, Y. B.; Song, J.-K.; Choi, S.; Lee, D. J.; Kim, J. H.; Lee, M.; Hyeon, T.; Kim, D.-H. Transparent and stretchable interactive human machine interface based on patterned graphene heterostructures. *Adv. Funct. Mater.* **2015**, *25* (3), 375−383.

(20) Xia, F.; Wang, H.; Jia, Y. Rediscovering black phosphorus as an anisotropic layered material for optoelectronics and electronics. *Nat. Commun.* **2014**, *5* (1), 1−6.

(21) Kim, M. K.; Parasuraman, R. N.; Wang, L.; Park, Y.; Kim, B.; Lee, S. J.; Lu, N.; Min, B.-C.; Lee, C. H. Soft-packaged sensory glove system for human-like natural interaction and control of prosthetic hands. *NPG Asia Mater.* **2019**, *11* (1), 1−12.

(22) Kaltenbrunner, M.; Sekitani, T.; Reeder, J.; Yokota, T.; Kuribara, K.; Tokuhara, T.; Drack, M.; Schwodiauer, R.; Graz, I.; Bauer-Gogonea, S.; Bauer, S.; Someya, T. An ultra-lightweight design for imperceptible plastic electronics. *Nature* **2013**, *499* (7459), 458−463.

(23) Rim, Y. S.; Bae, S. H.; Chen, H.; De Marco, N.; Yang, Y. Recent progress in materials and devices toward printable and flexible sensors. *Adv. Mater.* **2016**, *28* (22), 4415−4440.

(24) Yao, H. B.; Ge, J.; Wang, C. F.; Wang, X.; Hu, W.; Zheng, Z. J.; Ni, Y.; Yu, S. H. A flexible and highly pressure-sensitive graphene−polyurethane sponge based on fractured microstructure design. *Adv. Mater.* **2013**, *25* (46), 6692−6698.

(25) Liu, M.; Pu, X.; Jiang, C.; Liu, T.; Huang, X.; Chen, L.; Du, C.; Sun, J.; Hu, W.; Wang, Z. L. Large-area all-textile pressure sensors for monitoring human motion and physiological signals. *Adv. Mater.* **2017**, *29* (41), 1703700.

(26) Zhou, K.; Zhang, C.; Xiong, Z.; Chen, H. Y.; Li, T.; Ding, G.; Yang, B.; Liao, Q.; Zhou, Y.; Han, S. T. Template-Directed Growth of Hierarchical MOF Hybrid Arrays for Tactile Sensor. *Adv. Funct. Mater.* **2020**, *30* (38), 2001296.

(27) Ruth, S. R. A.; Beker, L.; Tran, H.; Feig, V. R.; Matsuhisa, N.; Bao, Z. Rational design of capacitive pressure sensors based on pyramidal microstructures for specialized monitoring of biosignals. *Adv. Funct. Mater.* **2020**, *30*, 1903100.

(28) Hu, L.; Kim, H. S.; Lee, J.-Y.; Peumans, P.; Cui, Y. Scalable coating and properties of transparent, flexible, silver nanowire electrodes. *ACS Nano* **2010**, *4* (5), 2955−2963.

(29) Yang, Y.; Guan, L.; Li, X.; Gao, Z.; Ren, X.; Gao, G. Conductive organohydrogels with ultrastretchability, antifreezing, self-healing, and adhesive properties for motion detection and signal transmission. *ACS Appl. Mater. Interfaces* **2019**, *11* (3), 3428−3437.

(30) Li, X.; Yang, T.; Yang, Y.; Zhu, J.; Li, L.; Alam, F. E.; Li, X.; Wang, K.; Cheng, H.; Lin, C.-T.; Fang, Y.; Zhu, H. Large-area ultrathin graphene films by single-step marangoni self-assembly for highly sensitive strain sensing application. *Adv. Funct. Mater.* **2016**, *26* (9), 1322−1329.

(31) Yang, J.; Luo, S.; Zhou, X.; Li, J.; Fu, J.; Yang, W.; Wei, D. Flexible, tunable, and ultrasensitive capacitive pressure sensor with microconformal graphene electrodes. *ACS Appl. Mater. Interfaces* **2019**, *11* (16), 14997−15006.

(32) Xu, M.; Gao, Y.; Yu, G.; Lu, C.; Tan, J.; Xuan, F. Flexible pressure sensor using carbon nanotube-wrapped polydimethylsiloxane microspheres for tactile sensing. *Sens. Actuators, A* **2018**, *284*, 260−265.

(33) Yuan, Z.; Zhou, T.; Yin, Y.; Cao, R.; Li, C.; Wang, Z. L. Transparent and flexible triboelectric sensing array for touch security applications. *ACS Nano* **2017**, *11* (8), 8364−8369.

(34) Yang, J. C.; Kim, J.-O.; Oh, J.; Kwon, S. Y.; Sim, J. Y.; Kim, D. W.; Choi, H. B.; Park, S. Microstructured porous pyramid-based ultrahigh sensitive pressure sensor insensitive to strain and temperature. *ACS Appl. Mater. Interfaces* **2019**, *11* (21), 19472−19480.

(35) Jang, K.-I.; Li, K.; Chung, H. U.; Xu, S.; Jung, H. N.; Yang, Y.; Kwak, J. W.; Jung, H. H.; Song, J.; Yang, C. Self-assembled three dimensional network designs for soft electronics. *Nat. Commun.* **2017**, *8* (1), 1−10.

(36) Wang, X.; Que, M.; Chen, M.; Han, X.; Li, X.; Pan, C.; Wang, Z. L. Full Dynamic-Range Pressure Sensor Matrix Based on Optical and Electrical Dual-Mode Sensing. *Adv. Mater.* **2017**, *29* (15), 1605817.

(37) Tian, L.; Zimmerman, B.; Akhtar, A.; Yu, K. J.; Moore, M.; Wu, J.; Larsen, R. J.; Lee, J. W.; Li, J.; Liu, Y. Large-area MRI-compatible epidermal electronic interfaces for prosthetic control and cognitive monitoring. *Nat. Biomed. Eng.* **2019**, *3* (3), 194−205.

(38) Lu, Y.; Jiang, K.; Chen, D.; Shen, G. Wearable sweat monitoring system with integrated micro-supercapacitors. *Nano Energy* **2019**, *58*, 624−632.

(39) Huang, Z.; Hao, Y.; Li, Y.; Hu, H.; Wang, C.; Nomoto, A.; Pan, T.; Gu, Y.; Chen, Y.; Zhang, T. Three-dimensional integrated stretchable electronics. *Nat. Electron.* **2018**, *1* (8), 473−480.

(40) Yang, Z.; Xu, Q.; Wang, X.; Lu, J.; Wang, H.; Li, F.; Zhang, L.; Hu, G.; Pan, C. Large and Ultrastable All-Inorganic CsPbBr3 Monocrystalline Films: Low-Temperature Growth and Application for High-Performance Photodetectors. *Adv. Mater.* **2018**, *30* (44), 1802110.

(41) He, X.; Li, D.; Zhou, J.; Wang, W.; Xuan, W.; Dong, S.; Jin, H.; Luo, J. High sensitivity humidity sensors using flexible surface acoustic wave devices made on nanocrystalline ZnO/polyimide substrates. *J. Mater. Chem. C* **2013**, *1* (39), 6210−6215.

(42) Yang, T.; Xie, D.; Li, Z.; Zhu, H. Recent advances in wearable tactile sensors: Materials, sensing mechanisms, and device performance. *Mater. Sci. Eng., R* **2017**, *115*, 1−37.

(43) Chen, S.; Lou, Z.; Chen, D.; Shen, G. An artificial flexible visual memory system based on an UV-motivated Memristor. *Adv. Mater.* **2018**, *30* (7), 1705400.

(44) Zhao, S.; Wang, J.; Du, X.; Wang, J.; Cao, R.; Yin, Y.; Zhang, X.; Yuan, Z.; Xing, Y.; Pui, D. Y. H.; Li, C. All-nanofiber-based ultralight stretchable triboelectric nanogenerator for self-powered wearable electronics. *ACS Appl. Energy Mater.* **2018**, *1* (5), 2326−2332.

(45) Yuan, Z.; Du, X.; Niu, H.; Li, N.; Shen, G.; Li, C.; Wang, Z. L. Motion recognition by a liquid filled tubular triboelectric nano-generator. *Nanoscale* **2019**, *11* (2), 495−503.

(46) Li, G.; Qiu, Z.; Wang, Y.; Hong, Y.; Wan, Y.; Zhang, J.; Yang, J.; Wu, Z.; Hong, W.; Guo, C. F. PEDOT: PSS/grafted-PDMS electrodes for fully organic and intrinsically stretchable skin-like electronics. *ACS Appl. Mater. Interfaces* **2019**, *11* (10), 10373−10379.

(47) Liu, H.-S.; Pan, B.-C.; Liou, G.-S. Highly transparent AgNW/PDMS stretchable electrodes for elastomeric electrochromic devices. *Nanoscale* **2017**, *9* (7), 2633−2639.

(48) Jeong, S. H.; Zhang, S.; Hjort, K.; Hilborn, J.; Wu, Z. PDMS-based elastomer tuned soft, stretchable, and sticky for epidermal electronics. *Adv. Mater.* **2016**, *28* (28), 5830−5836.

(49) Güder, F.; Ainla, A.; Redston, J.; Mosadegh, B.; Glavan, A.; Martin, T.; Whitesides, G. M. Paper-based electrical respiration sensor. *Angew. Chem., Int. Ed.* **2016**, *55* (19), 5727−5732.

(50) Wang, C.; Li, X.; Gao, E.; Jian, M.; Xia, K.; Wang, Q.; Xu, Z.; Ren, T.; Zhang, Y. Carbonized silk fabric for ultrastretchable, highly sensitive, and wearable strain sensors. *Adv. Mater.* **2016**, *28* (31), 6640−6648.

(51) Nie, B.; Huang, R.; Yao, T.; Zhang, Y.; Miao, Y.; Liu, C.; Liu, J.; Chen, X. Textile-Based Wireless Pressure Sensor Array for Human-Interactive Sensing. *Adv. Funct. Mater.* **2019**, *29* (22), 1808786.

(52) Lund, A.; van der Velden, N. M.; Persson, N.-K.; Hamedi, M. M.; Müller, C. Electrically conducting fibres for e-textiles: An open playground for conjugated polymers and carbon nanomaterials. *Mater. Sci. Eng., R* **2018**, *126*, 1−29.

(53) Zhang, M.; Wang, C.; Wang, Q.; Jian, M.; Zhang, Y. Sheath−core graphite/silk fiber made by dry-meyer-rod-coating for wearable strain sensors. *ACS Appl. Mater. Interfaces* **2016**, *8* (32), 20894−20899.

(54) Jeon, J. W.; Cho, S. Y.; Jeong, Y. J.; Shin, D. S.; Kim, N. R.; Yun, Y. S.; Kim, H.-T.; Choi, S. B.; Hong, W. G.; Kim, H. J.; Jin, H.-J.; Kim, B. H. Pyroprotein-based electronic textiles with high stability. *Adv. Mater.* **2017**, *29* (6), 1605479.

(55) Hua, Q.; Liu, H.; Zhao, J.; Peng, D.; Yang, X.; Gu, L.; Pan, C. Bioinspired Electronic Whisker Arrays by Pencil-Drawn Paper for Adaptive Tactile Sensing. *Adv. Electron. Mater.* **2016**, *2* (7), 1600093.

(56) Yang, P.-K.; Lin, Z.-H.; Pradel, K. C.; Lin, L.; Li, X.; Wen, X.; He, J.-H.; Wang, Z. L. based origami triboelectric nanogenerators and self-powered pressure sensors. *ACS Nano* **2015**, *9* (1), 901−907.

(57) Yin, M.-J.; Yin, Z.; Zhang, Y.; Zheng, Q.; Zhang, A. P. Micropatterned elastic ionic polyacrylamide hydrogel for low-voltage capacitive and organic thin-film transistor pressure sensors. *Nano Energy* **2019**, *58*, 96−104.

(58) Yao, G.; Xu, L.; Cheng, X.; Li, Y.; Huang, X.; Guo, W.; Liu, S.; Wang, Z. L.; Wu, H. Bioinspired triboelectric nanogenerators as self-powered electronic skin for robotic tactile sensing. *Adv. Funct. Mater.* **2020**, *30* (6), 1907312.

(59) Rogers, J.; Lagally, M.; Nuzzo, R. Synthesis, assembly and applications of semiconductor nanomembranes. *Nature* **2011**, *477* (7362), 45−53.

(60) Liu, C.-H.; Yu, X. Silver nanowire-based transparent, flexible, and conductive thin film. *Nanoscale Res. Lett.* **2011**, *6* (1), 1−8.

(61) Tolvanen, J.; Hannu, J.; Jantunen, H. Stretchable and washable strain sensor based on cracking structure for human motion monitoring. *Sci. Rep.* **2018**, *8* (1), 1−10.

(62) Yang, Y.; Liu, J.; Cao, J.; Zhou, Z.; Zhang, X. A naturally-derived supramolecular elastomer containing green-synthesized silver nanofibers for self-repairing E-skin sensor. *J. Mater. Chem. C* **2019**, *7* (3), 578−585.

(63) Heo, Y.; Hwang, Y.; Jung, H. S.; Choa, S. H.; Ko, H. C. J. S. Secondary Sensitivity Control of Silver-Nanowire-Based Resistive-Type Strain Sensors by Geometric Modulation of the Elastomer Substrate. *Small* **2017**, *13* (23), 1700070.

(64) Jin, H.; Matsuhisa, N.; Lee, S.; Abbas, M.; Yokota, T.; Someya, T. Enhancing the performance of stretchable conductors for e-textiles by controlled ink permeation. *Adv. Mater.* **2017**, *29* (21), 1605848.

(65) Karthik, P.; Singh, S. P. Conductive silver inks and their applications in printed and flexible electronics. *RSC Adv.* **2015**, *5* (95), 77760−77790.

(66) Langley, D.; Giusti, G.; Mayousse, C.; Celle, C.; Bellet, D.; Simonato, J.-P. Flexible transparent conductive materials based on silver nanowire networks: a review. *Nanotechnology* **2013**, *24* (45), 452001.

(67) Li, B.; Ye, S.; Stewart, I. E.; Alvarez, S.; Wiley, B. J. Synthesis and purification of silver nanowires to make conducting films with a transmittance of 99%. *Nano Lett.* **2015**, *15* (10), 6722−6726.

(68) Sun, Y.; Xia, Y. Large-scale synthesis of uniform silver nanowires through a soft, self-seeding, polyol process. *Adv. Mater.* **2002**, *14* (11), 833−837.

(69) Yang, C.; Gu, H.; Lin, W.; Yuen, M. M.; Wong, C. P.; Xiong, M.; Gao, B. J. A. m. Silver nanowires: from scalable synthesis to recyclable foldable electronics. *Adv. Mater.* **2011**, *23* (27), 3052−3056.

(70) Liang, J.; Tong, K.; Pei, Q. A water-based silver-nanowire screen-print ink for the fabrication of stretchable conductors and wearable thin-film transistors. *Adv. Mater.* **2016**, *28* (28), 5986−5996.

(71) Liu, X.; Zhang, F.; Huang, R.; Pan, C.; Zhu, J. Capping Modes in PVP-Directed Silver Nanocrystal Growth: Multi-Twinned Nano-rods versus Single-Crystalline Nano-Hexapods. *Cryst. Growth Des.* **2008**, *8* (6), 1916−1923.

(72) Lin, S.; Bai, X.; Wang, H.; Wang, H.; Song, J.; Huang, K.; Wang, C.; Wang, N.; Li, B.; Lei, M.; Wu, H. Roll-to-Roll production of transparent silver-nanofiber-network electrodes for flexible electro-chromic smart windows. *Adv. Mater.* **2017**, *29* (41), 1703238.

(73) Huang, Y.; Bai, X.; Zhou, M.; Liao, S.; Yu, Z.; Wang, Y.; Wu, H. Large-scale spinning of silver nanofibers as flexible and reliable conductors. *Nano Lett.* **2016**, *16* (9), 5846−5851.

(74) Wu, H.; Kong, D.; Ruan, Z.; Hsu, P.-C.; Wang, S.; Yu, Z.; Carney, T. J.; Hu, L.; Fan, S.; Cui, Y. A transparent electrode based on a metal nanotrough network. *Nat. Nanotechnol.* **2013**, *8* (6), 421−425.

(75) Cai, L.; Song, A. Y.; Wu, P.; Hsu, P.-C.; Peng, Y.; Chen, J.; Liu, C.; Catrysse, P. B.; Liu, Y.; Yang, A.; Zhou, C.; Zhou, C.; Fan, S.; Cui, Y. Warming up human body by nanoporous metallized polyethylene textile. *Nat. Commun.* **2017**, *8* (1), 1−8.

(76) Lee, J.; Lee, P.; Lee, H.; Lee, D.; Lee, S. S.; Ko, S. H. Very long Ag nanowire synthesis and its application in a highly transparent, conductive and flexible metal electrode touch panel. *Nanoscale* **2012**, *4* (20), 6408−6414.

(77) Garnett, E. C.; Cai, W.; Cha, J. J.; Mahmood, F.; Connor, S. T.; Greyson Christoforo, M.; Cui, Y.; McGehee, M. D.; Brongersma, M. L. Self-limited plasmonic welding of silver nanowire junctions. *Nat. Mater.* **2012**, *11* (3), 241−249.

(78) Lu, H.; Zhang, D.; Ren, X.; Liu, J.; Choy, W. C. H. Selective Growth and Integration of Silver Nanoparticles on Silver Nanowires at Room Conditions for Transparent Nano-Network Electrode. *ACS Nano* **2014**, *8* (10), 10980−10987.

(79) Triambulo, R. E.; Cheong, H.-G.; Park, J.-W. All-solution-processed foldable transparent electrodes of Ag nanowire mesh and metal matrix films for flexible electronics. *Org. Electron.* **2014**, *15* (11), 2685−2695.

(80) Zhang, Z.; Zhang, X.; Xin, Z.; Deng, M.; Wen, Y.; Song, Y. Synthesis of monodisperse silver nanoparticles for ink-jet printed flexible electronics. *Nanotechnology* **2011**, *22* (42), 425601.

(81) Ahn, B. Y.; Lorang, D. J.; Lewis, J. A. J. A. m. Transparent conductive grids via direct writing of silver nanoparticle inks. *Nanoscale* **2011**, *3* (7), 2700−2702.

(82) Kim, T.; Kim, Y. W.; Lee, H. S.; Kim, H.; Yang, W. S.; Suh, K. S. Uniformly interconnected silver-nanowire networks for transparent film heaters. *Adv. Funct. Mater.* **2013**, *23* (10), 1250−1255.

(83) Kim, Y.; Zhu, J.; Yeom, B.; Di Prima, M.; Su, X.; Kim, J.-G.; Yoo, S. J.; Uher, C.; Kotov, N. A. Stretchable nanoparticle conductors with self-organized conductive pathways. *Nature* **2013**, *500* (7460), 59−63.

(84) Matsuhisa, N.; Inoue, D.; Zalar, P.; Jin, H.; Matsuba, Y.; Itoh, A.; Yokota, T.; Hashizume, D.; Someya, T. Printable elastic conductors by in situ formation of silver nanoparticles from silver flakes. *Nat. Mater.* **2017**, *16* (8), 834−840.

(85) Liao, X.; Zhang, Z.; Kang, Z.; Gao, F.; Liao, Q.; Zhang, Y. Ultrasensitive and stretchable resistive strain sensors designed for wearable electronics. *Mater. Horiz.* **2017**, *4* (3), 502−510.

(86) Zhu, B.; Gong, S.; Cheng, W. Softening gold for elastronics. *Chem. Soc. Rev.* **2019**, *48* (6), 1668−1711.

(87) Huo, Z.; Tsung, C.-k.; Huang, W.; Zhang, X.; Yang, P. Sub-two nanometer single crystal Au nanowires. *Nano Lett.* **2008**, *8* (7), 2041−2044.

(88) Maurer, J. H.; González-García, L.; Reiser, B.; Kanelidis, I.; Kraus, T. Templated self-assembly of ultrathin gold nanowires by nanoimprinting for transparent flexible electronics. *Nano Lett.* **2016**, *16* (5), 2921−2925.

(89) Fan, Z.; Huang, X.; Han, Y.; Bosman, M.; Wang, Q.; Zhu, Y.; Liu, Q.; Li, B.; Zeng, Z.; Wu, J.; Shi, W.; Li, S.; Gan, C. L.; Zhang, H. Surface modification-induced phase transformation of hexagonal close-packed gold square sheets. *Nat. Commun.* **2015**, *6* (1), 1−9.

(90) He, J.; Wang, Y.; Feng, Y.; Qi, X.; Zeng, Z.; Liu, Q.; Teo, W. S.; Gan, C. L.; Zhang, H.; Chen, H. Forest of gold nanowires: a new type of nanocrystal growth. *ACS Nano* **2013**, *7* (3), 2733−2740.

(91) Chen, L.; Ji, F.; Xu, Y.; He, L.; Mi, Y.; Bao, F.; Sun, B.; Zhang, X.; Zhang, Q. High-yield seedless synthesis of triangular gold nanoplates through oxidative etching. *Nano Lett.* **2014**, *14* (12), 7201−7206.

(92) Miyamoto, A.; Lee, S.; Cooray, N. F.; Lee, S.; Mori, M.; Matsuhisa, N.; Jin, H.; Yoda, L.; Yokota, T.; Itoh, A.; Sekino, M.; Kawasaki, H.; Ebihara, T.; Amagai, M.; Someya, T. Inflammation-free, gas-permeable, lightweight, stretchable on-skin electronics with nanomeshes. *Nat. Nanotechnol.* **2017**, *12* (9), 907.

(93) Wu, Y.; Mechael, S. S.; Chen, Y.; Carmichael, T. B. Solution deposition of conformal gold coatings on knitted fabric for e-textiles and electroluminescent clothing. *Adv. Mater. Technol.-US* **2018**, *3* (3), 1700292.

(94) Choi, S.; Han, S. I.; Jung, D.; Hwang, H. J.; Lim, C.; Bae, S.; Park, O. K.; Tschabrunn, C. M.; Lee, M.; Bae, S. Y. Highly conductive, stretchable and biocompatible Ag−Au core−sheath nanowire composite for wearable and implantable bioelectronics. *Nat. Nanotechnol.* **2018**, *13* (11), 1048−1056.

(95) Im, H.-G.; Jung, S.-H.; Jin, J.; Lee, D.; Lee, J.; Lee, D.; Lee, J.-Y.; Kim, I.-D.; Bae, B.-S. Flexible transparent conducting hybrid film using a surface-embedded copper nanowire network: a highly oxidation-resistant copper nanowire electrode for flexible optoelectronics. *ACS Nano* **2014**, *8* (10), 10973−10979.

(96) Yang, X.; Hu, X.; Wang, Q.; Xiong, J.; Yang, H.; Meng, X.; Tan, L.; Chen, L.; Chen, Y. Large-scale stretchable semiembedded copper nanowire transparent conductive films by an electrospinning template. *ACS Appl. Mater. Interfaces* **2017**, *9* (31), 26468−26475.

(97) Zhang, Y.; Guo, J.; Xu, D.; Sun, Y.; Yan, F. Synthesis of ultralong copper nanowires for high-performance flexible transparent conductive electrodes: the effects of polyhydric alcohols. *Langmuir* **2018**, *34* (13), 3884−3893.

(98) Zhang, D.; Wang, R.; Wen, M.; Weng, D.; Cui, X.; Sun, J.; Li, H.; Lu, Y. Synthesis of ultralong copper nanowires for high-performance transparent electrodes. *J. Am. Chem. Soc.* **2012**, *134* (35), 14283−14286.

(99) Jason, N. N.; Shen, W.; Cheng, W. Copper nanowires as conductive ink for low-cost draw-on electronics. *ACS Appl. Mater. Interfaces* **2015**, *7* (30), 16760−16766.

(100) Mehta, R.; Chugh, S.; Chen, Z. Enhanced Electrical and Thermal Conduction in Graphene-Encapsulated Copper Nanowires. *Nano Lett.* **2015**, *15* (3), 2024−2030.

(101) Chen, Z.; Ye, S.; Stewart, I. E.; Wiley, B. J. Copper Nanowire Networks with Transparent Oxide Shells That Prevent Oxidation without Reducing Transmittance. *ACS Nano* **2014**, *8* (9), 9673−9679.

(102) Rathmell, A. R.; Nguyen, M.; Chi, M.; Wiley, B. J. Synthesis of Oxidation-Resistant Cupronickel Nanowires for Transparent Conducting Nanowire Networks. *Nano Lett.* **2012**, *12* (6), 3193−3199.

(103) Hsu, P.-C.; Wu, H.; Carney, T. J.; McDowell, M. T.; Yang, Y.; Garnett, E. C.; Li, M.; Hu, L.; Cui, Y. Passivation Coating on Electrospun Copper Nanofibers for Stable Transparent Electrodes. *ACS Nano* **2012**, *6* (6), 5150−5156.

(104) Bhagavathi Kandy, S.; Simon, G. P.; Cheng, W.; Zank, J.; Saito, K.; Bhattacharyya, A. R. Effect of Organic Modification on Multiwalled Carbon Nanotube Dispersions in Highly Concentrated Emulsions. *ACS Omega* **2019**, *4* (4), 6647−6659.

(105) Hashempour, M.; Vicenzo, A.; Zhao, F.; Bestetti, M. Direct growth of MWCNTs on 316 stainless steel by chemical vapor deposition: Effect of surface nano-features on CNT growth and structure. *Carbon* **2013**, *63*, 330−347.

(106) Chen, K.; Gao, W.; Emaminejad, S.; Kiriya, D.; Ota, H.; Nyein, H. Y. Y.; Takei, K.; Javey, A. Printed carbon nanotube electronics and sensor systems. *Adv. Mater.* **2016**, *28* (22), 4397−4414.

(107) Zhang, R.; Zhang, Y.; Zhang, Q.; Xie, H.; Qian, W.; Wei, F. Growth of half-meter long carbon nanotubes based on Schulz−Flory distribution. *ACS Nano* **2013**, *7* (7), 6156−6161.

(108) Bai, Y.; Yue, H.; Wang, J.; Shen, B.; Sun, S.; Wang, S.; Wang, H.; Li, X.; Xu, Z.; Zhang, R.; Wei, F. Super-durable ultralong carbon nanotubes. *Science* **2020**, *369* (6507), 1104−1106.

(109) Sekitani, T.; Nakajima, H.; Maeda, H.; Fukushima, T.; Aida, T.; Hata, K.; Someya, T. Stretchable active-matrix organic light-emitting diode display using printable elastic conductors. *Nat. Mater.* **2009**, *8* (6), 494−499.

(110) Lipomi, D. J.; Vosgueritchian, M.; Tee, B. C.; Hellstrom, S. L.; Lee, J. A.; Fox, C. H.; Bao, Z. Skin-like pressure and strain sensors based on transparent elastic films of carbon nanotubes. *Nat. Nanotechnol.* **2011**, *6* (12), 788−792.

(111) Kholghi Eshkalak, S.; Chinnappan, A.; Jayathilaka, W.A.D.M.; Khatibzadeh, M.; Kowsari, E.; Ramakrishna, S. A review on inkjet printing of CNT composites for smart applications. *Appl. Mater. Today* **2017**, *9*, 372−386.

(112) Urper, O.; Çakmak, İ.; Karatepe, N. Fabrication of carbon nanotube transparent conductive films by vacuum filtration method. *Mater. Lett.* **2018**, *223*, 210−214.

(113) Kim, J.-O.; Kwon, S. Y.; Kim, Y.; Choi, H. B.; Yang, J. C.; Oh, J.; Lee, H. S.; Sim, J. Y.; Ryu, S.; Park, S. Highly ordered 3d microstructure-based electronic skin capable of differentiating pressure, temperature, and proximity. *ACS Appl. Mater. Interfaces* **2019**, *11* (1), 1503−1511.

(114) Son, D.; Kang, J.; Vardoulis, O.; Kim, Y.; Matsuhisa, N.; Oh, J. Y.; To, J. W.; Mun, J.; Katsumata, T.; Liu, Y. An integrated self-healable electronic skin system fabricated via dynamic reconstruction of a nanostructured conducting network. *Nat. Nanotechnol.* **2018**, *13* (11), 1057−1065.

(115) Zheng, Q.; Ip, W. H.; Lin, X.; Yousefi, N.; Yeung, K. K.; Li, Z.; Kim, J.-K. Transparent conductive films consisting of ultralarge graphene sheets produced by Langmuir−Blodgett assembly. *ACS Nano* **2011**, *5* (7), 6039−6051.

(116) Idrees, M.; Batool, S.; Kong, J.; Zhuang, Q.; Liu, H.; Shao, Q.; Lu, N.; Feng, Y.; Wujcik, E. K.; Gao, Q.; Ding, T.; Wei, R.; Guo, Z. Polyborosilazane derived ceramics-nitrogen sulfur dual doped graphene nanocomposite anode for enhanced lithium ion batteries. *Electrochim. Acta* **2019**, *296*, 925−937.

(117) Han, M. Y.; Özyilmaz, B.; Zhang, Y.; Kim, P. Energy band-gap engineering of graphene nanoribbons. *Phys. Rev. Lett.* **2007**, *98* (20), 206805.

(118) Zhu, G.; Cui, X.; Zhang, Y.; Chen, S.; Dong, M.; Liu, H.; Shao, Q.; Ding, T.; Wu, S.; Guo, Z. Poly (vinyl butyral)/graphene oxide/poly (methylhydrosiloxane) nanocomposite coating for improved aluminum alloy anticorrosion. *Polymer* **2019**, *172*, 415−422.

(119) Zhang, Y.; An, Y.; Wu, L.; Chen, H.; Li, Z.; Dou, H.; Murugadoss, V.; Fan, J.; Zhang, X.; Mai, X.; Guo, Z. Metal-free energy storage systems: combining batteries with capacitors based on a methylene blue functionalized graphene cathode. *J. Mater. Chem. A* **2019**, *7* (34), 19668−19675.

(120) Tour, J. M. x. Top-down versus bottom-up fabrication of graphene-based electronics. *Chem. Mater.* **2014**, *26* (1), 163−171.

(121) Zheng, Q.; Li, Z.; Yang, J.; Kim, J.-K. Graphene oxide-based transparent conductive films. *Prog. Mater. Sci.* **2014**, *64*, 200−247.

(122) Torrisi, F.; Hasan, T.; Wu, W.; Sun, Z.; Lombardo, A.; Kulmala, T. S.; Hsieh, G.-W.; Jung, S.; Bonaccorso, F.; Paul, P. J.; Chu, D.; Ferrari, A. C. Inkjet-printed graphene electronics. *ACS Nano* **2012**, *6* (4), 2992−3006.

(123) Robinson, J. T.; Zalalutdinov, M.; Baldwin, J. W.; Snow, E. S.; Wei, Z.; Sheehan, P.; Houston, B. H. Wafer-scale reduced graphene oxide films for nanomechanical devices. *Nano Lett.* **2008**, *8* (10), 3441−3445.

(124) Wang, S. J.; Geng, Y.; Zheng, Q.; Kim, J.-K. Fabrication of highly conducting and transparent graphene films. *Carbon* **2010**, *48* (6), 1815−1823.

(125) Jakus, A. E.; Secor, E. B.; Rutz, A. L.; Jordan, S. W.; Hersam, M. C.; Shah, R. N. Three-dimensional printing of high-content graphene scaffolds for electronic and biomedical applications. *ACS Nano* **2015**, *9* (4), 4636−4648.

(126) Que, M.; Guo, W.; Zhang, X.; Li, X.; Hua, Q.; Dong, L.; Pan, C. Flexible quantum dot-sensitized solar cells employing CoS nanorod arrays/graphite paper as effective counter electrodes. *J. Mater. Chem. A* **2014**, *2* (33), 13661−13666.

(127) Hensleigh, R. M.; Cui, H.; Oakdale, J. S.; Ye, J. C.; Campbell, P. G.; Duoss, E. B.; Spadaccini, C. M.; Zheng, X.; Worsley, M. A. Additive manufacturing of complex micro-architected graphene aerogels. *Mater. Horiz.* **2018**, *5* (6), 1035−1041.

(128) Sha, J.; Li, Y.; Villegas Salvatierra, R.; Wang, T.; Dong, P.; Ji, Y.; Lee, S.-K.; Zhang, C.; Zhang, J.; Smith, R. H.; Ajayan, P. M.; Lou, J.; Zhao, N.; Tour, J. M. Three-dimensional printed graphene foams. *ACS Nano* **2017**, *11* (7), 6860−6867.

(129) Zheng, Q.; Liu, X.; Xu, H.; Cheung, M.-S.; Choi, Y.-W.; Huang, H.-C.; Lei, H.-Y.; Shen, X.; Wang, Z.; Wu, Y.; Kim, S. Y.; Kim, J.-K. Sliced graphene foam films for dual-functional wearable strain sensors and switches. *Nanoscale Horiz* **2018**, *3* (1), 35−44.

(130) Guo, Y.; Ruan, K.; Yang, X.; Ma, T.; Kong, J.; Wu, N.; Zhang, J.; Gu, J.; Guo, Z. Constructing fully carbon-based fillers with a hierarchical structure to fabricate highly thermally conductive polyimide nanocomposites. *J. Mater. Chem. C* **2019**, *7* (23), 7035−7044.

(131) Chen, J.; Yu, Q.; Cui, X.; Dong, M.; Zhang, J.; Wang, C.; Fan, J.; Zhu, Y.; Guo, Z. An overview of stretchable strain sensors from conductive polymer nanocomposites. *J. Mater. Chem. C* **2019**, *7* (38), 11710−11730.

(132) Chen, T.; Dai, L. Carbon nanomaterials for high-performance supercapacitors. *Mater. Today* **2013**, *16* (7−8), 272−280.

(133) Shen, X.; Wang, Z.; Wu, Y.; Liu, X.; He, Y.-B.; Zheng, Q.; Yang, Q.-H.; Kang, F.; Kim, J.-K. A three-dimensional multilayer graphene web for polymer nanocomposites with exceptional transport properties and fracture resistance. *Mater. Horiz.* **2018**, *5* (2), 275−284.

(134) Huang, X.; Sun, B.; Su, D.; Zhao, D.; Wang, G. Soft-template synthesis of 3D porous graphene foams with tunable architectures for lithium−O 2 batteries and oil adsorption applications. *J. Mater. Chem. A* **2014**, *2* (21), 7973−7979.

(135) Estevez, L.; Kelarakis, A.; Gong, Q.; Da'as, E. H.; Giannelis, E. P. Multifunctional graphene/platinum/nafion hybrids via ice templating. *J. Am. Chem. Soc.* **2011**, *133* (16), 6122−6125.

(136) Xu, Y.; Sheng, K.; Li, C.; Shi, G. Self-assembled graphene hydrogel via a one-step hydrothermal process. *ACS Nano* **2010**, *4* (7), 4324−4330.

(137) Huang, C.; Bai, H.; Li, C.; Shi, G. J. C. C. A graphene oxide/hemoglobin composite hydrogel for enzymatic catalysis in organic solvents. *Chem. Commun.* **2011**, *47* (17), 4962−4964.

(138) Chun, S.; Kim, Y.; Jin, H.; Choi, E.; Lee, S.-B.; Park, W. A graphene force sensor with pressure-amplifying structure. *Carbon* **2014**, *78*, 601−608.

(139) Huang, C. B.; Witomska, S.; Aliprandi, A.; Stoeckel, M. A.; Bonini, M.; Ciesielski, A.; Samorì, P. Molecule−graphene hybrid materials with tunable mechanoresponse: highly sensitive pressure sensors for health monitoring. *Adv. Mater.* **2019**, *31* (1), 1804600.

(140) Zhou, K.; Chen, C.; Lei, M.; Gao, Q.; Nie, S.; Liu, X.; Wang, S. Reduced graphene oxide-based highly sensitive pressure sensor for wearable electronics via an ordered structure and enhanced interlayer interaction mechanism. *RSC Adv.* **2020**, *10* (4), 2150−2159.

(141) Lou, Z.; Chen, S.; Wang, L.; Jiang, K.; Shen, G. J. A. M. An ultra-sensitive and rapid response speed graphene pressure sensors for electronic skin and health monitoring. *Nano Energy* **2016**, *23*, 7−14.

(142) Pang, Y.; Zhang, K.; Yang, Z.; Jiang, S.; Ju, Z.; Li, Y.; Wang, X.; Wang, D.; Jian, M.; Zhang, Y.; Liang, R.; Tian, H.; Yang, Y.; Ren, T.-L. Epidermis microstructure inspired graphene pressure sensor with random distributed spinosum for high sensitivity and large linearity. *ACS Nano* **2018**, *12* (3), 2346−2354.

(143) Rivnay, J.; Inal, S.; Collins, B. A.; Sessolo, M.; Stavrinidou, E.; Strakosas, X.; Tassone, C.; Delongchamp, D. M.; Malliaras, G. G. Structural control of mixed ionic and electronic transport in conducting polymers. *Nat. Commun.* **2016**, *7* (1), 1−9.

(144) Stavrinidou, E.; Leleux, P.; Rajaona, H.; Khodagholy, D.; Rivnay, J.; Lindau, M.; Sanaur, S.; Malliaras, G. G. Direct measurement of ion mobility in a conducting polymer. *Adv. Mater.* **2013**, *25* (32), 4488−4493.

(145) Tahk, D.; Lee, H. H.; Khang, D.-Y. Elastic moduli of organic electronic materials by the buckling method. *Macromolecules* **2009**, *42* (18), 7079−7083.

(146) Wang, Y.; Zhu, C.; Pfattner, R.; Yan, H.; Jin, L.; Chen, S.; Molina-Lopez, F.; Lissel, F.; Liu, J.; Rabiah, N. I.; Chen, Z.; Chung, J. W.; Linder, C.; Toney, M. F.; Murmann, B.; Bao, Z. A highly stretchable, transparent, and conductive polymer. *Sci. Adv.* **2017**, *3* (3), No. e1602076.

(147) Oh, J. Y.; Kim, S.; Baik, H. K.; Jeong, U. Conducting polymer dough for deformable electronics. *Adv. Mater.* **2016**, *28* (22), 4455−4461.

(148) Liu, Y.; Liu, J.; Chen, S.; Lei, T.; Kim, Y.; Niu, S.; Wang, H.; Wang, X.; Foudeh, A. M.; Tok, J. B.-H.; Bao, Z. Soft and elastic hydrogel-based microelectronics for localized low-voltage neuro-modulation. *Nat. Biomed. Eng.* **2019**, *3* (1), 58−68.

(149) Lee, W.; Kim, D.; Matsuhisa, N.; Nagase, M.; Sekino, M.; Malliaras, G. G.; Yokota, T.; Someya, T. Transparent, conformable, active multielectrode array using organic electrochemical transistors. *Proc. Natl. Acad. Sci. U. S. A.* **2017**, *114* (40), 10554−10559.

(150) Khodagholy, D.; Doublet, T.; Quilichini, P.; Gurfinkel, M.; Leleux, P.; Ghestem, A.; Ismailova, E.; Herve, T.; Sanaur, S.; Bernard, C.; Malliaras, G. G. In vivo recordings of brain activity using organic transistors. *Nat. Commun.* **2013**, *4* (1), 1−7.

(151) Seliktar, D. Designing cell-compatible hydrogels for biomedical applications. *Science* **2012**, *336* (6085), 1124−1128.

(152) Carreras, P.; Chaves, R. C.; Gallardo, M.; Ortiz, A.; Lopez, J. M.; Sia, S. K. Microengineering double layer hydrogel structures towards the recapitulation of the hematopoietic stem cell niche. *Sci. Bull.* **2018**, *63* (20), 1319−1323.

(153) Yang, Y.; Guan, L.; Li, X.; Gao, Z.; Ren, X.; Gao, G. Conductive organohydrogels with ultrastretchability, antifreezing, self-healing, and adhesive properties for motion detection and signal transmission. *ACS Appl. Mater. Interfaces* **2019**, *11* (3), 3428−3437.

(154) Parida, K.; Kumar, V.; Jiangxin, W.; Bhavanasi, V.; Bendi, R.; Lee, P. S. Highly transparent, stretchable, and self-healing ionic-skin

triboelectric nanogenerators for energy harvesting and touch applications. *Adv. Mater.* **2017**, *29* (37), 1702181.

(155) Sheng, H.; Wang, X.; Kong, N.; Xi, W.; Yang, H.; Wu, X.; Wu, K.; Li, C.; Hu, J.; Tang, J.; Zhou, J.; Duan, S.; Wang, H.; Suo, Z. Neural interfaces by hydrogels. *Extreme Mech. Lett.* **2019**, *30*, 100510.

(156) Haraguchi, K.; Takehisa, T. Nanocomposite hydrogels: A unique organic−inorganic network structure with extraordinary mechanical, optical, and swelling/de-swelling properties. *Adv. Mater.* **2002**, *14* (16), 1120−1124.

(157) Sun, J.-Y.; Zhao, X.; Illeperuma, W. R.; Chaudhuri, O.; Oh, K. H.; Mooney, D. J.; Vlassak, J. J.; Suo, Z. Highly stretchable and tough hydrogels. *Nature* **2012**, *489* (7414), 133−136.

(158) Green, R. A.; Lovell, N. H.; Wallace, G. G.; Poole-Warren, L. A. Conducting polymers for neural interfaces: challenges in developing an effective long-term implant. *Biomaterials* **2008**, *29* (24−25), 3393−3399.

(159) Green, R.; Abidian, M. R. Conducting polymers for neural prosthetic and neural interface applications. *Adv. Mater.* **2015**, *27* (46), 7620−7637.

(160) Feig, V. R.; Tran, H.; Lee, M.; Bao, Z. Mechanically tunable conductive interpenetrating network hydrogels that mimic the elastic moduli of biological tissue. *Nat. Commun.* **2018**, *9* (1), 1−9.

(161) Duan, J.; Liang, X.; Guo, J.; Zhu, K.; Zhang, L. Ultra-stretchable and force-sensitive hydrogels reinforced with chitosan microspheres embedded in polymer networks. *Adv. Mater.* **2016**, *28* (36), 8037−8044.

(162) Rogers, J. A.; Someya, T.; Huang, Y. Materials and mechanics for stretchable electronics. *Science* **2010**, *327* (5973), 1603−1607.

(163) Kim, D. H.; Rogers, J. A. Bend, Buckle, and Fold: Mechanical Engineering with Nanomembranes. *ACS Nano* **2009**, *3* (3), 498−501.

(164) Mickle, A. D.; Won, S. M.; Noh, K. N.; Yoon, J.; Meacham, K. W.; Xue, Y.; McIlvried, L. A.; Copits, B. A.; Samineni, V. K.; Crawford, K. E. A wireless closed-loop system for optogenetic peripheral neuromodulation. *Nature* **2019**, *565* (7739), 361−365.

(165) Yan, Z.; Pan, T.; Xue, M.; Chen, C.; Cui, Y.; Yao, G.; Huang, L.; Liao, F.; Jing, W.; Zhang, H.; Gao, M.; Guo, D.; Xia, Y.; Lin, Y. Thermal release transfer printing for stretchable conformal bioelectronics. *Adv. Sci.* **2017**, *4* (11), 1700251.

(166) Yoo, J.; Jeong, S.; Kim, S.; Je, J. H. A stretchable nanowire UV−vis−NIR photodetector with high performance. *Adv. Mater.* **2015**, *27* (10), 1712−1717.

(167) Dickey, M. D. Stretchable and soft electronics using liquid metals. *Adv. Mater.* **2017**, *29* (27), 1606425.

(168) Zhu, Y. Mechanics of crystalline nanowires: an experimental perspective. *Appl. Mech. Rev.* **2017**, *69* (1), 010802.

(169) Hwang, B.-U.; Lee, J.-H.; Trung, T. Q.; Roh, E.; Kim, D.-I.; Kim, S.-W.; Lee, N.-E. Transparent stretchable self-powered patchable sensor platform with ultrasensitive recognition of human activities. *ACS Nano* **2015**, *9* (9), 8801−8810.

(170) Kim, D. H.; Xiao, J.; Song, J.; Huang, Y.; Rogers, J. A. Stretchable, curvilinear electronics based on inorganic materials. *Adv. Mater.* **2010**, *22* (19), 2108−2124.

(171) Naserifar, N.; LeDuc, P. R.; Fedder, G. K. Material gradients in stretchable substrates toward integrated electronic functionality. *Adv. Mater.* **2016**, *28* (18), 3584−3591.

(172) Mohan, A. V.; Kim, N.; Gu, Y.; Bandodkar, A. J.; You, J. M.; Kumar, R.; Kurniawan, J. F.; Xu, S.; Wang, J. Merging of Thin-and Thick-Film Fabrication Technologies: Toward Soft Stretchable "Island−Bridge" Devices. *Adv. Mater. Technol.-US* **2017**, *2* (4), 1600284.

(173) Choi, S.; Lee, H.; Ghaffari, R.; Hyeon, T.; Kim, D. H. Recent advances in flexible and stretchable bio-electronic devices integrated with nanomaterials. *Adv. Mater.* **2016**, *28* (22), 4203−4218.

(174) Huang, Q.; Zhu, Y. Gravure printing of water-based silver nanowire ink on plastic substrate for flexible electronics. *Sci. Rep.* **2018**, *8* (1), 1−10.

(175) Li, R.; Li, M.; Su, Y.; Song, J.; Ni, X. An analytical mechanics model for the island-bridge structure of stretchable electronics. *Soft Matter* **2013**, *9* (35), 8476−8482.

(176) Yang, S.; Ng, E.; Lu, N. Indium Tin Oxide (ITO) serpentine ribbons on soft substrates stretched beyond 100. *Extreme Mech. Lett.* **2015**, *2*, 37−45.

(177) Alcheikh, N.; Shaikh, S. F.; Hussain, M. M. J. E. M. L. Ultra-stretchable Archimedean interconnects for stretchable electronics. *Extreme Mech. Lett.* **2018**, *24*, 6−13.

(178) Xu, S.; Yan, Z.; Jang, K.-I.; Huang, W.; Fu, H.; Kim, J.; Wei, Z.; Flavin, M.; McCracken, J.; Wang, R. J. S. Assembly of micro/nanomaterials into complex, three-dimensional architectures by compressive buckling. *Science* **2015**, *347* (6218), 154−159.

(179) Ma, Q.; Zhang, Y. Mechanics of fractal-inspired horseshoe microstructures for applications in stretchable electronics. *J. Appl. Mech.* **2016**, *83* (11), 111008.

(180) Zhang, Y.; Fu, H.; Xu, S.; Fan, J. A.; Hwang, K.-C.; Jiang, J.; Rogers, J. A.; Huang, Y. A hierarchical computational model for stretchable interconnects with fractal-inspired designs. *J. Mech. Phys. Solids* **2014**, *72*, 115−130.

(181) Tang, Y.; Lin, G.; Yang, S.; Yi, Y. K.; Kamien, R. D.; Yin, J. Programmable Kiri-Kirigami Metamaterials. *Adv. Mater.* **2017**, *29* (10), 1604262.

(182) Callens, S. J.; Zadpoor, A. A. From flat sheets to curved geometries: Origami and kirigami approaches. *Mater. Today* **2018**, *21* (3), 241−264.

(183) Wang, G.-J. N.; Zheng, Y.; Zhang, S.; Kang, J.; Wu, H.-C.; Gasperini, A.; Zhang, H.; Gu, X.; Bao, Z. Tuning the cross-linker crystallinity of a stretchable polymer semiconductor. *Chem. Mater.* **2019**, *31* (17), 6465−6475.

(184) Mun, J.; Wang, G.-J. N.; Oh, J. Y.; Katsumata, T.; Lee, F. L.; Kang, J.; Wu, H.-C.; Lissel, F.; Rondeau-Gagne, S.; Tok, J. B.-H.; Bao, Z. Effect of nonconjugated spacers on mechanical properties of semiconducting polymers for stretchable transistors. *Adv. Funct. Mater.* **2018**, *28* (43), 1804222.

(185) Xu, F.; Wu, M.-Y.; Safron, N. S.; Roy, S. S.; Jacobberger, R. M.; Bindl, D. J.; Seo, J.-H.; Chang, T.-H.; Ma, Z.; Arnold, M. S. Highly stretchable carbon nanotube transistors with ion gel gate dielectrics. *Nano Lett.* **2014**, *14* (2), 682−686.

(186) Kim, H.-J.; Sim, K.; Thukral, A.; Yu, C. Rubbery electronics and sensors from intrinsically stretchable elastomeric composites of semiconductors and conductors. *Sci. Adv.* **2017**, *3* (9), No. e1701114.

(187) Wang, S.; Xu, J.; Wang, W.; Wang, G.-J. N.; Rastak, R.; Molina-Lopez, F.; Chung, J. W.; Niu, S.; Feig, V. R.; Lopez, J.; Lei, T.; Kwon, S.-K.; Kim, Y.; Foudeh, A. M.; Ehrlich, A.; Gasperini, A.; Yun, Y.; Murmann, B.; Tok, J. B.-H.; Bao, Z. Skin electronics from scalable fabrication of an intrinsically stretchable transistor array. *Nature* **2018**, *555* (7694), 83−88.

(188) Xu, S.; Zhang, Y.; Cho, J.; Lee, J.; Huang, X.; Jia, L.; Fan, J. A.; Su, Y.; Su, J.; Zhang, H. Stretchable batteries with self-similar serpentine interconnects and integrated wireless recharging systems. *Nat. Commun.* **2013**, *4* (1), 1−8.

(189) Amjadi, M.; Kyung, K. U.; Park, I.; Sitti, M. Stretchable, skin-mountable, and wearable strain sensors and their potential applications: a review. *Adv. Funct. Mater.* **2016**, *26* (11), 1678−1698.

(190) Ruth, S. R. A.; Feig, V. R.; Tran, H.; Bao, Z. Microengineering Pressure Sensor Active Layers for Improved Performance. *Adv. Funct. Mater.* **2020**, *30* (39), 2003491.

(191) Yu, G.; Hu, J.; Tan, J.; Gao, Y.; Lu, Y.; Xuan, F. A wearable pressure sensor based on ultra-violet/ozone microstructured carbon nanotube/polydimethylsiloxane arrays for electronic skins. *Nanotechnology* **2018**, *29* (11), 115502.

(192) Zhao, T.; Li, T.; Chen, L.; Yuan, L.; Li, X.; Zhang, J. Highly Sensitive Flexible Piezoresistive Pressure Sensor Developed Using Biomimetically Textured Porous Materials. *ACS Appl. Mater. Interfaces* **2019**, *11* (32), 29466−29473.

(193) Xu, M.; Gao, Y.; Yu, G.; Lu, C.; Tan, J.; Xuan, F. Flexible pressure sensor using carbon nanotube-wrapped polydimethylsiloxane microspheres for tactile sensing. *Sens. Actuators, A* **2018**, *284*, 260−265.

(194) Li, H.; Wu, K.; Xu, Z.; Wang, Z.; Meng, Y.; Li, L. Ultrahigh-sensitivity piezoresistive pressure sensors for detection of tiny pressure. *ACS Appl. Mater. Interfaces* **2018**, *10* (24), 20826−20834.

(195) Gao, Y.; Lu, C.; Guohui, Y.; Sha, J.; Tan, J.; Xuan, F. Laser micro-structured pressure sensor with modulated sensitivity for electronic skins. *Nanotechnology* **2019**, *30* (32), 325502.

(196) Peng, S.; Blanloeuil, P.; Wu, S.; Wang, C. H. Rational design of ultrasensitive pressure sensors by tailoring microscopic features. *Adv. Mater. Interfaces* **2018**, *5* (18), 1800403.

(197) Shi, J.; Wang, L.; Dai, Z.; Zhao, L.; Du, M.; Li, H.; Fang, Y. Multiscale hierarchical design of a flexible piezoresistive pressure sensor with high sensitivity and wide linearity range. *Small* **2018**, *14* (27), 1800819.

(198) Yang, J. C.; Kim, J.-O.; Oh, J.; Kwon, S. Y.; Sim, J. Y.; Kim, D. W.; Choi, H. B.; Park, S. Microstructured porous pyramid-based ultrahigh sensitive pressure sensor insensitive to strain and temperature. *ACS Appl. Mater. Interfaces* **2019**, *11* (21), 19472−19480.

(199) Visser, C. W.; Amato, D. N.; Mueller, J.; Lewis, J. A. Architected polymer foams via direct bubble writing. *Adv. Mater.* **2019**, *31* (46), 1904668.

(200) Wang, Z.; Zhang, L.; Liu, J.; Jiang, H.; Li, C. Flexible hemispheric microarrays of highly pressure-sensitive sensors based on breath figure method. *Nanoscale* **2018**, *10* (22), 10691−10698.

(201) Wei, Y.; Chen, S.; Lin, Y.; Yang, Z.; Liu, L. Cu−Ag core−shell nanowires for electronic skin with a petal molded microstructure. *J. Mater. Chem. C* **2015**, *3* (37), 9594−9602.

(202) Ruth, S. R. A.; Beker, L.; Tran, H.; Feig, V. R.; Matsuhisa, N.; Bao, Z. Rational design of capacitive pressure sensors based on pyramidal microstructures for specialized monitoring of biosignals. *Adv. Funct. Mater.* **2020**, *30*, 1903100.

(203) Mannsfeld, S. C.; Tee, B. C.; Stoltenberg, R. M.; Chen, C. V. H.; Barman, S.; Muir, B. V.; Sokolov, A. N.; Reese, C.; Bao, Z. J. N. m. Highly sensitive flexible pressure sensors with microstructured rubber dielectric layers. *Nat. Mater.* **2010**, *9* (10), 859−864.

(204) Tee, B. C. K.; Chortos, A.; Dunn, R. R.; Schwartz, G.; Eason, E.; Bao, Z. Tunable flexible pressure sensors using microstructured elastomer geometries for intuitive electronics. *Adv. Funct. Mater.* **2014**, *24* (34), 5427−5434.

(205) Bae, G. Y.; Han, J. T.; Lee, G.; Lee, S.; Kim, S. W.; Park, S.; Kwon, J.; Jung, S.; Cho, K. Pressure/temperature sensing bimodal electronic skin with stimulus discriminability and linear sensitivity. *Adv. Mater.* **2018**, *30* (43), 1803388.

(206) Xiong, Y.; Shen, Y.; Tian, L.; Hu, Y.; Zhu, P.; Sun, R.; Wong, C.-P. A flexible, ultra-highly sensitive and stable capacitive pressure sensor with convex microarrays for motion and health monitoring. *Nano Energy* **2020**, *70*, 104436.

(207) Joo, Y.; Byun, J.; Seong, N.; Ha, J.; Kim, H.; Kim, S.; Kim, T.; Im, H.; Kim, D.; Hong, Y. Silver nanowire-embedded PDMS with a multiscale structure for a highly sensitive and robust flexible pressure sensor. *Nanoscale* **2015**, *7* (14), 6208−6215.

(208) Huang, Y.-C.; Liu, Y.; Ma, C.; Cheng, H.-C.; He, Q.; Wu, H.; Wang, C.; Lin, C.-Y.; Huang, Y.; Duan, X. Sensitive pressure sensors based on conductive microstructured air-gap gates and two-dimensional semiconductor transistors. *Nat. Electron.* **2020**, *3* (1), 59−69.

(209) Cheng, M.-Y.; Lin, C.-L.; Lai, Y.-T.; Yang, Y.-J. A polymer-based capacitive sensing array for normal and shear force measurement. *Sensors* **2010**, *10* (11), 10211−10225.

(210) Kang, S.; Lee, J.; Lee, S.; Kim, S.; Kim, J. K.; Algadi, H.; Al-Sayari, S.; Kim, D. E.; Kim, D.; Lee, T. Highly sensitive pressure sensor based on bioinspired porous structure for real-time tactile sensing. *Adv. Electron. Mater.* **2016**, *2* (12), 1600356.

(211) Amjadi, M.; Pichitpajongkit, A.; Lee, S.; Ryu, S.; Park, I. Highly stretchable and sensitive strain sensor based on silver nanowire−elastomer nanocomposite. *ACS Nano* **2014**, *8* (5), 5154−5163.

(212) Alamusi; Hu, N.; Fukunaga, H.; Atobe, S.; Liu, Y.; Li, J. Piezoresistive strain sensors made from carbon nanotubes based polymer nanocomposites. *Sensors* **2011**, *11* (11), 10691−10723.

(213) Wang, C.; Zhao, J.; Ma, C.; Sun, J.; Tian, L.; Li, X.; Li, F.; Han, X.; Liu, C.; Shen, C.; Dong, L.; Yang, J.; Pan, C. Detection of non-joint areas tiny strain and anti-interference voice recognition by micro-cracked metal thin film. *Nano Energy* **2017**, *34*, 578−585.

(214) Yan, C.; Wang, J.; Kang, W.; Cui, M.; Wang, X.; Foo, C. Y.; Chee, K. J.; Lee, P. S. Highly stretchable piezoresistive graphene−nanocellulose nanopaper for strain sensors. *Adv. Mater.* **2014**, *26* (13), 2022−2027.

(215) Liu, Q.; Chen, J.; Li, Y.; Shi, G. High-performance strain sensors with fish-scale-like graphene-sensing layers for full-range detection of human motions. *ACS Nano* **2016**, *10* (8), 7901−7906.

(216) Pang, C.; Lee, C.; Suh, K. Y. Recent advances in flexible sensors for wearable and implantable devices. *J. Appl. Polym. Sci.* **2013**, *130* (3), 1429−1441.

(217) Wang, Y.; Wang, L.; Yang, T.; Li, X.; Zang, X.; Zhu, M.; Wang, K.; Wu, D.; Zhu, H. Wearable and highly sensitive graphene strain sensors for human motion monitoring. *Adv. Funct. Mater.* **2014**, *24* (29), 4666−4670.

(218) Park, J. J.; Hyun, W. J.; Mun, S. C.; Park, Y. T.; Park, O. O. Highly stretchable and wearable graphene strain sensors with controllable sensitivity for human motion monitoring. *ACS Appl. Mater. Interfaces* **2015**, *7* (11), 6317−6324.

(219) Gong, S.; Lai, D. T.; Su, B.; Si, K. J.; Ma, Z.; Yap, L. W.; Guo, P.; Cheng, W. Highly stretchy black gold E-skin nanopatches as highly sensitive wearable biomedical sensors. *Adv. Electron. Mater.* **2015**, *1* (4), 1400063.

(220) Wang, X.; Qiu, Y.; Cao, W.; Hu, P. Highly stretchable and conductive core−sheath chemical vapor deposition graphene fibers and their applications in safe strain sensors. *Chem. Mater.* **2015**, *27* (20), 6969−6975.

(221) Cai, L.; Song, L.; Luan, P.; Zhang, Q.; Zhang, N.; Gao, Q.; Zhao, D.; Zhang, X.; Tu, M.; Yang, F.; Zhou, W.; Fan, Q.; Luo, J.; Zhou, W.; Ajayan, P. M.; Xie, S. Super-stretchable, transparent carbon nanotube-based capacitive strain sensors for human motion detection. *Sci. Rep.* **2013**, *3* (1), 1−9.

(222) Cohen, D. J.; Mitra, D.; Peterson, K.; Maharbiz, M. M. A highly elastic, capacitive strain gauge based on percolating nanotube networks. *Nano Lett.* **2012**, *12* (4), 1821−1825.

(223) Im, H.; Kim, T.; Song, H.; Choi, J.; Park, J. S.; Ovalle-Robles, R.; Yang, H. D.; Kihm, K. D.; Baughman, R. H.; Lee, H. H.; Kang, T. J.; Kim, Y. H. High-efficiency electrochemical thermal energy harvester using carbon nanotube aerogel sheet electrodes. *Nat. Commun.* **2016**, *7* (1), 1−9.

(224) Fan, F. R.; Tang, W.; Wang, Z. L. Flexible nanogenerators for energy harvesting and self-powered electronics. *Adv. Mater.* **2016**, *28* (22), 4283−4305.

(225) Pan, C.; Luo, Z.; Xu, C.; Luo, J.; Liang, R.; Zhu, G.; Wu, W.; Guo, W.; Yan, X.; Xu, J.; Wang, Z. L.; Zhu, J. Wafer-Scale High-Throughput Ordered Arrays of Si and Coaxial Si/Si1−xGex Wires: Fabrication, Characterization, and Photovoltaic Application. *ACS Nano* **2011**, *5* (8), 6629−6636.

(226) Du, W.; Han, X.; Lin, L.; Chen, M.; Li, X.; Pan, C.; Wang, Z. L. A Three Dimensional Multi-Layered Sliding Triboelectric Nanogenerator. *Adv. Energy Mater.* **2014**, *4* (11), 1301592.

(227) Sun, J.; Pu, X.; Jiang, C.; Du, C.; Liu, M.; Zhang, Y.; Liu, Z.; Zhai, J.; Hu, W.; Wang, Z. L. Self-powered electrochromic devices with tunable infrared intensity. *Sci. Bull.* **2018**, *63* (12), 795−801.

(228) Nshimyimana, E.; Su, X.; Xie, H.; Liu, W.; Deng, R.; Luo, T.; Yan, Y.; Tang, X. Realization of non-equilibrium process for high thermoelectric performance Sb-doped GeTe. *Sci. Bull.* **2018**, *63* (11), 717−725.

(229) Wang, Z. L. Triboelectric nanogenerators as new energy technology and self-powered sensors−Principles, problems and perspectives. *Faraday Discuss.* **2014**, *176*, 447−458.

(230) Wang, Z. L.; Zhu, G.; Yang, Y.; Wang, S.; Pan, C. Progress in nanogenerators for portable electronics. *Mater. Today* **2012**, *15* (12), 532−543.

(231) Ding, W.; Wang, A. C.; Wu, C.; Guo, H.; Wang, Z. L. Human−machine interfacing enabled by triboelectric nanogenerators and tribotronics. *Adv. Mater. Technol.-US* **2019**, *4* (1), 1800487.

(232) Wang, Z. L. On Maxwell's displacement current for energy and sensors: the origin of nanogenerators. *Mater. Today* **2017**, *20* (2), 74−82.

(233) Wei, X. Y.; Wang, X.; Kuang, S. Y.; Su, L.; Li, H. Y.; Wang, Y.; Pan, C.; Wang, Z. L.; Zhu, G. Dynamic Triboelectrification-Induced Electroluminescence and its Use in Visualized Sensing. *Adv. Mater.* **2016**, *28* (31), 6656−6664.

(234) Pu, X.; Liu, M.; Chen, X.; Sun, J.; Du, C.; Zhang, Y.; Zhai, J.; Hu, W.; Wang, Z. L. Ultrastretchable, transparent triboelectric nanogenerator as electronic skin for biomechanical energy harvesting and tactile sensing. *Sci. Adv.* **2017**, *3* (5), No. e1700015.

(235) Wu, C.; Ding, W.; Liu, R.; Wang, J.; Wang, A. C.; Wang, J.; Li, S.; Zi, Y.; Wang, Z. L. Keystroke dynamics enabled authentication and identification using triboelectric nanogenerator array. *Mater. Today* **2018**, *21* (3), 216−222.

(236) Wang, X.; Zhang, H.; Dong, L.; Han, X.; Du, W.; Zhai, J.; Pan, C.; Wang, Z. L. Self-powered high-resolution and pressure-sensitive triboelectric sensor matrix for real-time tactile mapping. *Adv. Mater.* **2016**, *28* (15), 2896−2903.

(237) Hong, S. Y.; Lee, Y. H.; Park, H.; Jin, S. W.; Jeong, Y. R.; Yun, J.; You, I.; Zi, G.; Ha, J. S. Stretchable active matrix temperature sensor array of polyaniline nanofibers for electronic skin. *Adv. Mater.* **2016**, *28* (5), 930−935.

(238) Wang, C.; Hwang, D.; Yu, Z.; Takei, K.; Park, J.; Chen, T.; Ma, B.; Javey, A. User-interactive electronic skin for instantaneous pressure visualization. *Nat. Mater.* **2013**, *12* (10), 899−904.

(239) Sun, Q.; Seung, W.; Kim, B. J.; Seo, S.; Kim, S. W.; Cho, J. H. Active matrix electronic skin strain sensor based on piezopotential-powered graphene transistors. *Adv. Mater.* **2015**, *27* (22), 3411−3417.

(240) Choi, M.; Park, Y. J.; Sharma, B. K.; Bae, S.-R.; Kim, S. Y.; Ahn, J.-H. Flexible active-matrix organic light-emitting diode display enabled by MoS2 thin-film transistor. *Sci. Adv.* **2018**, *4* (4), No. eaas8721.

(241) Yao, S.; Zhu, Y. Wearable multifunctional sensors using printed stretchable conductors made of silver nanowires. *Nanoscale* **2014**, *6* (4), 2345−2352.

(242) Wang, X.; Zhang, Y.; Zhang, X.; Huo, Z.; Li, X.; Que, M.; Peng, Z.; Wang, H.; Pan, C. A highly stretchable transparent self-powered triboelectric tactile sensor with metallized nanofibers for wearable electronics. *Adv. Mater.* **2018**, *30* (12), 1706738.

(243) Zhao, X.; Hua, Q.; Yu, R.; Zhang, Y.; Pan, C. Flexible, stretchable and wearable multifunctional sensor array as artificial electronic skin for static and dynamic strain mapping. *Adv. Electron. Mater.* **2015**, *1* (7), 1500142.

(244) Peng, Y.; Que, M.; Lee, H. E.; Bao, R.; Wang, X.; Lu, J.; Yuan, Z.; Li, X.; Tao, J.; Sun, J.; Zhai, J.; Lee, K. J.; Pan, C. Achieving high-resolution pressure mapping via flexible GaN/ZnO nanowire LEDs array by piezo-phototronic effect. *Nano Energy* **2019**, *58*, 633−640.

(245) Wang, X.; Peng, D.; Huang, B.; Pan, C.; Wang, Z. L. Piezophotonic effect based on mechanoluminescent materials for advanced flexible optoelectronic applications. *Nano Energy* **2019**, *55*, 389−400.

(246) Qiao, S.; Liu, J.; Fu, G.; Ren, K.; Li, Z.; Wang, S.; Pan, C. ZnO nanowire based CIGS solar cell and its efficiency enhancement by the piezo-phototronic effect. *Nano Energy* **2018**, *49*, 508.

(247) Wang, C.; Bao, R.; Zhao, K.; Zhang, T.; Dong, L.; Pan, C. Enhanced emission intensity of vertical aligned flexible ZnO nanowire/p-polymer hybridized LED array by piezo-phototronic effect. *Nano Energy* **2015**, *14*, 364−371.

(248) Wen, X.; Wu, W.; Pan, C.; Hu, Y.; Yang, Q.; Lin Wang, Z. Development and progress in piezotronics. *Nano Energy* **2015**, *14*, 276−295.

(249) Hu, G.; Guo, W.; Yu, R.; Yang, X.; Zhou, R.; Pan, C.; Wang, Z. L. Enhanced performances of flexible ZnO/perovskite solar cells by piezo-phototronic effect. *Nano Energy* **2016**, *23*, 27−33.

(250) Pan, C.; Chen, M.; Yu, R.; Yang, Q.; Hu, Y.; Zhang, Y.; Wang, Z. L. Progress in Piezo-Phototronic-Effect-Enhanced Light-Emitting Diodes and Pressure Imaging. *Adv. Mater.* **2016**, *28* (8), 1535−1552.

(251) Harada, S.; Kanao, K.; Yamamoto, Y.; Arie, T.; Akita, S.; Takei, K. Fully printed flexible fingerprint-like three-axis tactile and slip force and temperature sensors for artificial skin. *ACS Nano* **2014**, *8* (12), 12851−12857.

(252) Kim, J.; Lee, M.; Shim, H. J.; Ghaffari, R.; Cho, H. R.; Son, D.; Jung, Y. H.; Soh, M.; Choi, C.; Jung, S.; Chu, K.; Jeon, D.; Lee, S.-T.; Kim, J. H.; Choi, S. H.; Hyeon, T.; Kim, D.-H. Stretchable silicon nanoribbon electronics for skin prosthesis. *Nat. Commun.* **2014**, *5* (1), 1−11.

(253) Ho, D. H.; Sun, Q.; Kim, S. Y.; Han, J. T.; Kim, D. H.; Cho, J. H. J. A. M. Stretchable and multimodal all graphene electronic skin. *Adv. Mater.* **2016**, *28* (13), 2601−2608.

(254) Trung, T. Q.; Ramasundaram, S.; Hwang, B. U.; Lee, N. E. An all-elastomeric transparent and stretchable temperature sensor for body-attachable wearable electronics. *Adv. Mater.* **2016**, *28* (3), 502−509.

(255) Xu, R.; Lee, J. W.; Pan, T.; Ma, S.; Wang, J.; Han, J. H.; Ma, Y.; Rogers, J. A.; Huang, Y. Designing thin, ultrastretchable electronics with stacked circuits and elastomeric encapsulation materials. *Adv. Funct. Mater.* **2017**, *27* (4), 1604545.

(256) Hua, Q.; Sun, J.; Liu, H.; Bao, R.; Yu, R.; Zhai, J.; Pan, C.; Wang, Z. L. Skin-inspired highly stretchable and conformable matrix networks for multifunctional sensing. *Nat. Commun.* **2018**, *9* (1), 1−11.

(257) Wang, C.; Sim, K.; Chen, J.; Kim, H.; Rao, Z.; Li, Y.; Chen, W.; Song, J.; Verduzco, R.; Yu, C. Soft ultrathin electronics innervated adaptive fully soft robots. *Adv. Mater.* **2018**, *30* (13), 1706695.

(258) Wan, C.; Chen, G.; Fu, Y.; Wang, M.; Matsuhisa, N.; Pan, S.; Pan, L.; Yang, H.; Wan, Q.; Zhu, L.; Chen, X. An artificial sensory neuron with tactile perceptual learning. *Adv. Mater.* **2018**, *30* (30), 1801291.

(259) Zhou, K.; Zhao, Y.; Sun, X.; Yuan, Z.; Zheng, G.; Dai, K.; Mi, L.; Pan, C.; Liu, C.; Shen, C. Ultra-stretchable triboelectric nanogenerator as high-sensitive and self-powered electronic skins for energy harvesting and tactile sensing. *Nano Energy* **2020**, *70*, 104546.

(260) Kim, D.; Kim, D.; Lee, H.; Jeong, Y. R.; Lee, S.-J.; Yang, G.; Kim, H.; Lee, G.; Jeon, S.; Zi, G.; Kim, J.; Ha, J. S. Body-attachable and stretchable multisensors integrated with wirelessly rechargeable energy storage devices. *Adv. Mater.* **2016**, *28* (4), 748−756.

(261) Sadri, B.; Goswami, D.; Sala de Medeiros, M.; Pal, A.; Castro, B.; Kuang, S.; Martinez, R. V. Wearable and implantable epidermal paper-based electronics. *ACS Appl. Mater. Interfaces* **2018**, *10* (37), 31061−31068.

(262) Honda, W.; Harada, S.; Arie, T.; Akita, S.; Takei, K. Wearable, human-interactive, health-monitoring, wireless devices fabricated by macroscale printing techniques. *Adv. Funct. Mater.* **2014**, *24* (22), 3299−3304.

(263) Li, J.; Bao, R.; Tao, J.; Dong, M.; Zhang, Y.; Fu, S.; Peng, D.; Pan, C. Visually aided tactile enhancement system based on ultrathin highly sensitive crack-based strain sensors. *Appl. Phys. Rev.* **2020**, *7* (1), 011404.

(264) Tao, J.; Dong, M.; Li, L.; Wang, C.; Li, J.; Liu, Y.; Bao, R.; Pan, C. Real-time pressure mapping smart insole system based on a controllable vertical pore dielectric layer. *Microsyst. Nanoeng.* **2020**, *6* (1), 1−10.